

國立臺灣大學理學院化學系

碩士論文

Department of Chemistry

College of Science

National Taiwan University

Master Thesis



二聚體中單重態激發分裂電子耦合之理論計算研究  
Theoretical Study on Singlet Fission Electronic Couplings  
in Dimer Systems

孫敬

Jing Sun

指導教授：鄭原忠博士

Advisor: Yuan-Chung Cheng, Ph.D.

中華民國 106 年 6 月

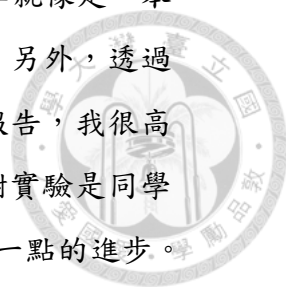
June, 2017



## 誌謝

和很多同學一樣，對於未知的選擇，我也曾經茫然過。回想當初大三選擇實驗室時，一時之間不知道該選哪個實驗室才好，每位教授所鑽研的方向不同，當時的我不知道該如何選擇向哪一位教授學習。在茫然的情況下，最後選擇加入我的導師的實驗室，但一段時間後發現，那並不是我想要的，誠然，當時導師給的方向很有趣，充滿了實際操作的部分，但我總覺得缺少了些什麼，最後發現，原來我一直不懂當時實驗成功或失敗的要求是什麼，我又能預期實驗有什麼變化，最後我得到的結論是我學的知識還不夠多，各種現象都有它背後的道理，而我卻知其然，而不知其所以然。在實驗中發生的現象，而我卻無法從過往的知識給出任何解釋，這也促使我想要多了解關於理論的知識。

很幸運的，之後我加入了鄭原忠老師的實驗室。在這裡，有別於以往在課堂上所學的知識，大大加了我對於同一問題的深度及廣度。不只如此，也改變了我對學習的態度。還記得一開始做專題時，由於是接上一位學長的工作，再加上做理論化學會用上終端機來進行運算，學長留下的資料是由C語言編成的，而當時的我並不會任何一點，因此不知該從何著手，當我把問題反應給鄭老師時，老師不疑有他的說，不會就自己學習，當下我頓時恍然大悟，雖然我以往有自習的習慣，但那是在有修克的情況下，但我也因此陷入誤區，認為修課是學習新東西的唯一方法。思慮過後便有了改正，到了現在，我可以自信的說我學會了C語言，並且我還學會了其他不同的電腦語言。在鄭老師的實驗室裡，我學到的不僅是豐富的知識，還有學習的態度以及處理問題的方式，因此我很感謝鄭原忠老師，讓我有機會加入老師的實驗室。



再來我也感謝實驗室和我一起學習的同學，每一位同學就像是一本書，有了大家的幫助，我的研究才得以有條不紊的進行。另外，透過每個禮拜三得中午，大家對自己有興趣的主題進行口頭報告，我很高興可以有更多的機會來進進口頭報告，更重要的是，感謝實驗是同學耐心的聽我講說，發表意見，讓我在口頭報告上可以一點一點的進步。最後我要感謝林仕凱學長，在研究的過程中，我遇到了許多困難，學長總是不厭其煩的撥出時間和我討論，之後還會持續關心我的問題是否已靜解決了，對此真心感謝學長對我的幫助。

當然我還要感謝我父母，在求學的路途中，一直支持我的決定，讓我掌控自己的人生，雖然父母無法在研究的過程給予幫助，在我休息得時候，默默的在我背後付出，讓我能安心的做研究。儘管我從未說出任何感謝的話，但我時常感謝的語言放在心裡，所以屆這個機會表達我對父母的感謝。

最後也謝謝台灣大學，謝謝扶輪社，我清楚知道一個人努力的背後，都有一群人在默默的幫助，我很感謝幫助過我的每一個人。



## 摘要

單重態分裂是一個描述分子在吸收到一個光子之後進而產生多個三重態激子的過程。這種過程由於被認為可以拿來應用在太陽能電池上而被大家所重視。雖然過去已有許多研究在討論單重態分裂，但是單重態分裂的反應機制仍然有所爭議，例如控制單重態分裂效率的條件和描述單重態分裂的激發態波函數等等。

從電子結構著手，我們利用非絕熱基底近似展示了激發態的性質。並且利用有限電子活躍空間的電子組態交互作用闡述了多組態在多并苯二聚體激發態的重要性。

藉由過去工作提到的三態模型，有效哈密頓量展示了基組的選取和電子活躍空間的大小對於電子耦合常數影響很小，但對於電子激發態的能量卻影響很大。在嘗試引入完全電子活躍空間的二階微擾理論之後，結果呈現之強電子耦合及近簡併的性質也解釋了單重態分裂的反應機制，也表示在靜態和動態相關能量之間取得平衡在共軛體系也是相當重要的。

最後，我們展示了二聚體中重要的有效電子耦合常數受到結構的影響。在二聚體中的有效電子耦合常數會和單體間的軌域重疊積分有著密切的關係，因此我們可以從單體間的重疊積分來得知分子間的相對方向會對單重態分裂的效率有什麼樣的影響。此方法也從分子結構方向的觀點提供了一個方向來設計高效單重態分裂的染料敏化太陽能電池。





# Abstract

Because of the promising potential in the high-efficiency solar cell, singlet exciton fission (SF), the molecular analog of multiexciton generation in which the absorption of one photon results in the generation of two triplet excitons, has attracted intensive research attention recently. Although the striking research are advancing, the mechanism of SF is still controversial, and some open questions remain, e.g., the key parameters manipulating the occurrence of SF and the excited state wavefunctions involved in it. From an electronic structure point of view, we construct an approximate diabatic basis to unambiguously interpret the character of the excited states, by applying the restricted active space equation of motion single and double approach to show the importance of considering multi-configurational effects in polyacene dimers. Using a three-state model, the effective hamiltonian shows that strong superexchange effective couplings depend on little on the choose of the basis set and the size of the active space while the diabatic state energies depend on a lot. Second order perturbation theory is introduced, the results show strong couplings and near degeneracy condition that explain the ultrafast SF mechanism, which shows striking the balance between static and dynamic correlation is also important in conjugated systems. Finally, we show that dominant effective couplings in a dimer system strongly correlated with the monomeric orbital overlap between two molecules. Hence, in a dimer system, the overlap between two monomers elucidate the dependence of the relative orientation of monomers on the efficiency of SF providing a criterion to the

design principle of high SF efficiency dye-sensitized cells.



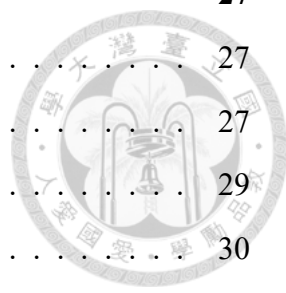


# Contents

口試委員會審定書	iii
誌謝	v
摘要	vii
<b>Abstract</b>	<b>ix</b>
<b>1 Introduction</b>	<b>1</b>
1.1 Singlet Fission . . . . .	1
1.2 Experimental Development . . . . .	2
1.3 Theoretical Development . . . . .	5
1.4 Outlook . . . . .	7
<b>2 Effective Singlet fission Hamiltonians from RAS-SD-EOM Calculations</b>	<b>9</b>
2.1 Properties of Electronic States in SF . . . . .	9
2.2 Localization of Molecular Orbitals . . . . .	10
2.3 Restricted Active Space Single and Double Equation of Motion (RAS-SD-EOM) Method . . . . .	11
2.4 Three-state Model . . . . .	13
2.5 Model Dimer Systems . . . . .	14
2.6 Basis Set Dependence of Effective Hamiltonian in Ethylene dimer . . . . .	15
2.7 Active Space Dependence of Hamiltonian . . . . .	18
2.8 Energy Correction by Second Order Perturbation Theory . . . . .	20



<b>3</b>	<b>The Dependence of Geometrical Change on Couplings</b>	<b>27</b>
3.1	SF Couplings and Orbital Overlaps . . . . .	27
3.1.1	Four-Electron-Four-Orbital Approximation . . . . .	27
3.1.2	Expansion of Configurational Couplings . . . . .	29
3.1.3	Approximation of Two Electron Integrals . . . . .	30
3.2	Effect of Slip Displacement . . . . .	31
3.2.1	Ethylene . . . . .	32
3.2.2	Tetracene . . . . .	34
3.2.3	Pyrene . . . . .	36
3.3	Effect of Relative Orientation . . . . .	37
3.4	Overlap as an Indicator of Couplings . . . . .	39
3.4.1	2D Mapping of the Overlap Integrals . . . . .	39
3.4.2	Overlap in Tetracene Crystalline Pair . . . . .	41
<b>4</b>	<b>Conclusion</b>	<b>45</b>
	<b>Bibliography</b>	<b>47</b>





# List of Figures

1.1	Illustration of the general model for singlet fission, where $\psi_g$ represent ground state while $\psi_{FE}$ , $\psi_{TT}$ and $\psi_T$ represent the frenkel exciton state, the multiexciton state and the triplet state, respectively. . . . .	3
2.1	Spin adapted configurations relevant to the singlet fission process problems. Red and blue are used to denote MOs belong to molecule A and B, respectively. . . . .	10
2.2	Illustration of block diagonalization of the truncated CI matrix. (FE block, CT block and the TT block) . . . . .	14
2.3	The three state model systems studied in this chapter (a) tetracene. (b) pentacene. The face-to-face distance is 3.7Å and the displacement of the slip in short axis is of 0.5Å. The nearest crystal pair of (c) pentacene. . . .	15
2.4	The dependence of basis set on (a) energy (b) coupling in ethylene dimer system. . . . .	17
2.5	The comparison of diabatic state energy of the effective hamiltonain which is constructed in different size of active space (a) tetracene model dimer (b) pentacene model dimer (c) pentacene crystalline dimer. . . . .	21
2.6	The comparison of couplings of the effective hamiltonain which is constructed in different size of active space (a) tetracene model dimer (b) pentacene model dimer (c) pentacene crystalline dimer. . . . .	22
2.7	The comparison of diabatic state energy corrected by CASPT2 with different size of active space included in effective hamiltonian (a) tetracene model dimer (b)pentacene model dimer (c) pentacene crystal. . . . .	25

3.1	Illustration of the slip displacement, where the yellow points are the centers of the ethylene monomers. . . . .	33
3.2	(a) Visualizations of HOMO and LUMO in ethylene monomer. The dependence of $\Delta x$ on (b) couplings, (c) two electron integrals and (d) overlap. Other parameters are $\Delta y = 0\text{\AA}$ and $\Delta z = 4.5\text{\AA}$ . . . . .	34
3.3	(a) Visualizations of HOMO and LUMO in tetracene monomer. The dependence of $\Delta y$ on (b) couplings, (c) two electron integrals and (d) overlap. Other parameters are $\Delta x = 0\text{\AA}$ and $\Delta z = 4\text{\AA}$ . . . . .	36
3.4	(a) Visualizations of HOMO and LUMO in pyrene monomer. The dependence of $\Delta x$ on (b) couplings, (c) two electron integrals and (d) overlap. Other parameters are $\Delta y = 0\text{\AA}$ and $\Delta z = 4\text{\AA}$ . . . . .	38
3.5	Comparisons of (a) overlap, (b) two electron integrals and (c) couplings in a face-to-face tetracene dimer with one monomer is rotated along long axis. Other parameters are $\Delta x = 0\text{\AA}$ , $\Delta y = 0\text{\AA}$ and $\Delta z = 4\text{\AA}$ . . . . .	39
3.6	Comparisons of (a) $\langle TT H CT\rangle$ , (b) $\langle S_1S_1 H CT\rangle$ and (c) $\langle h_B l_A\rangle$ , which are functions of $\Delta x$ and $\Delta y$ in ethylene dimer. Accordingly, (d), (e) and (f) in tetracene as well as (g), (h) and (i) in pyrene. The units of couplings are meV. . . . .	41
3.7	Illustration of a tetracene dimer with one monomer is rotated $\theta$ and shifted $\Delta y$ . Other parameters are $\Delta x = 0\text{\AA}$ and $\Delta z = 4\text{\AA}$ . . . . .	43
3.8	2-D mapping of $\langle h_B l_A\rangle$ in a tetracene dimer as functions $\theta$ and shifted $\Delta y$ . Other parameters are $\Delta x = 0\text{\AA}$ and $\Delta z = 4\text{\AA}$ . . . . .	43

# List of Tables







# Chapter 1

## Introduction

### 1.1 Singlet Fission

Singlet fission (SF) is a spin-allowed internal conversion process, in which a singlet exciton splits into two triplet excitons in a dimer system [1–4] as illustrated in Fig. 1.1. [5] The absorption of light induces the formation of the lowest-lying Frenkel exciton state ( $\psi_{FE}$ ), [6] which successively goes through a spin-allowed internal conversion to a multi-exciton dark state or called correlated triplet state ( $\psi_{TT}$ ). Finally, two independent triplet excitons form and diffuse away in the system as the dephasing of the coupled triplet excitons in the occurrence of the correlated triplet state.

From a mechanistic perspective, two types of models have been proposed to describe the process from  $\psi_{FE}$  to  $\psi_{TT}$ : (1) the direct mechanism, where  $\psi_{FE}$  is strongly coupled to  $\psi_{TT}$  giving rise to the ultrafast internal conversion. (2) the superexchange mechanism, where charge transfer state ( $\psi_{CT}$ ) mediates the ultrafast internal conversion from  $\psi_{FE}$  to  $\psi_{TT}$ . In general, SF process can be viewed as a special case of internal conversion and it has been observed in many materials.

SF process was observed in the 1960s in anthracene crystals and since then it was observed in many other systems such as tetracene, pentacene and perylene diimide crystals, etc. [1, 4, 7–16] Despite initial reports of singlet fission over 40 years ago, an explosion of experimental studies have emerged only recently due to the potential for photovoltaic utility. SF materials are expected to be applied to the solar cells for high efficiency, be-

cause SF process can be utilized to overcome the Shockley-Queisser limit [17, 18]. The Shockley-Queisser limit is described by Shockley and Queisser. They theoretically predicted that the maximal energy efficiency of a single junction solar cell is only about 31% because of the inaccessibility of photons whose energy are lower than the band gap, and the excessive energy of high-energy photons, which convert into wasted heat. [18]

The potential application of SF materials has attracted intensive research attention recently. Proposed by Nozik and coworkers in 2006, [19] with the application of SF material, the solar cell overcame the Shockley-Queisser limit by utilizing high-frequency part of solar energy to generate two electron-hole pairs from a single photon. In 2013, a singlet fission based organic photovoltaic cell achieving above 100% external quantum efficiency was reported and this further enlightens the promising applications of SF materials in the usage of solar energy. [17]

Recently, both theoretical and experimental results exert intensive effort to elucidate the mechanism of SF to shed light on the key parameters controlling the efficiency of SF, which are important for designing SF dye sensitizers. [5, 20–22] In the next sections, we will review previous experimental and theoretical works to provide a general background of interesting open problems in this field.

## 1.2 Experimental Development

SF was first probed by delayed fluorescence of anthracene crystal in the 60s. [1] Formed by SF, two independent triplet excitons have a chance to fuse into a singlet exciton with energy twice of the energy of the triplet exciton ( $E(\psi_T)$ ) via the up-conversion process. As a result, in addition to fluorescence emission from the singlet exciton pumped by the initial radiation, the successive appearance of a delayed fluorescence signal in the femtosecond time scale from the up conversion process was considered as an evidence of the occurrence of SF. However, the delayed fluorescence technique can not probe the ultrafast excited state dynamics of SF owing to the lack of ultrafast time resolution.

Recently, pump-probe transient absorption spectroscopy (TA) has been utilized to observe SF process in pentacene thin film. [23] The absorption around 620 nm in TA spec-

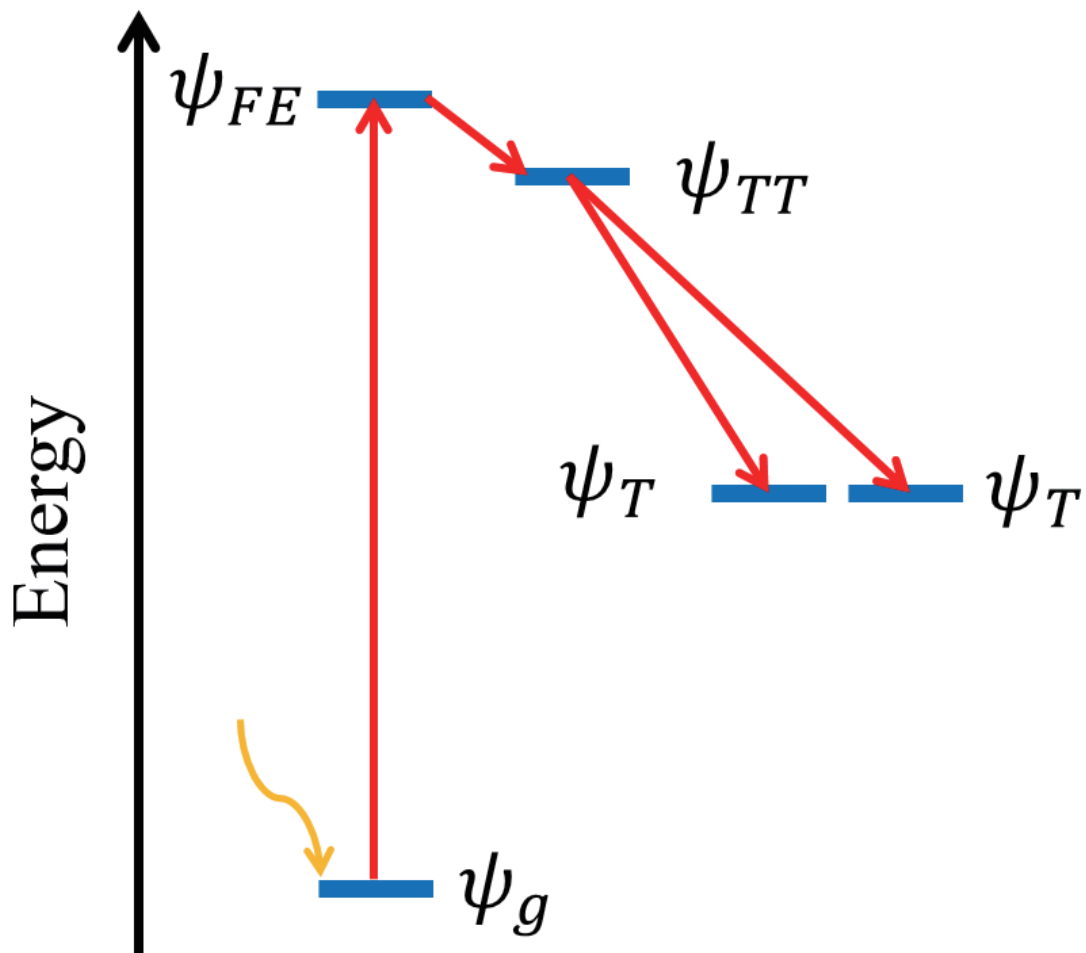


Figure 1.1: Illustration of the general model for singlet fission, where  $\psi_g$  represent ground state while  $\psi_{FE}$ ,  $\psi_{TT}$  and  $\psi_T$  represent the frenkel exciton state, the multiexciton state and the triplet state, respectively.



trum of pentacene thin film is denoted as the appearance of triplet excitons which support the occurrence of SF. The TA technique utilizes two laser pulses separated by the span of a delayed time, the former is called pumped pulse and the latter is probe pulse. [24] The ultrafast pump pulse first excites the system into the excited state, then for a given range of delayed time, the probe pulse, which is the white light continuum monitors the optical properties of the system. The ability to directly observe femtosecond excited state dynamics in SF brings the possibility of uncovering the mechanism of SF.

Moreover, the ultrafast appearance of triplet excitons supporting the occurrence of SF within femtosecond time scale in pentacene polycrystalline and thin film system has been demonstrated by several groups using the TA technique. [23–30] In addition, the molecular dimers of tetracene are studied by TA spectroscopy to confirm the occurrence of SF in covalently-linked dimer systems, making significant progress in the development of SF-based dye-sensitizing solar cell. [31]

In 2006, Müller et al. investigated the photophysical properties of bistetracene (1,4-bis(tetracene-5-yl)benzene) in benzene solution. Their results show that its steady-state spectroscopy is remarkably similar to that of monomeric tetracene, which means SF may not be observed in this system. Although TA spectrum shows that a small (<1%) fraction of the singlet excited states undergoes fission into two triplet states, the existence of SF suggests that it may be possible to optimize various aspects of the molecule's structure in order to enhance the fission rate and achieve triplet quantum yields greater than one. Since then, there have been other research successfully observing SF in other covalently linked tetracene dimer derivatives [32, 33], which also confirms that the structure of a linked dimer can be manipulated by the linkers.

Besides, the observation of SF process in the covalently linked pentacene and 1,3-diphenylisobenzofuran dimers in solution has shown that SF can be observed in other kinds of covalently linked dimer systems. [34, 35] Unlike the bistetracene which uses the benzene as a linker, the covalently linked pentacene dimers use non-conjugated 1,3-diethynyladamantyl spacer to manipulate the structure of the dimer. The non-conjugated linker is even more rigid than the benzene, which means the linked dimer can be fixed to

a specific structure by the non-conjugated linker. The utilization of the non-conjugated linker shows that we can further control the structure of the dimers.

For the covalently dimers, we can obtain the optimal dimer with high SF efficiency by choosing different monomers of the dimer system as well as manipulating the linkers to change the structure of the linked dimers. However, it is impossible to synthesize all different dimers and structures in order to find the optimal dimers with high SF efficiency. It is required to find a simple method to investigate the SF efficiency in different dimers and structures.

### 1.3 Theoretical Development

An obstacle to solar-energy applications is that high SF efficiency are found only in a few molecular systems, namely crystalline solids or aggregates of tetracene and pentacene. [36–39] A better understanding of the mechanisms of singlet fission is needed to guide the design and synthesis of materials with improved fission yields.

In 2010, to study the efficiency of SF, Ratner and coworkers emphasize the energy level matching between the lowest single excited state and  $\psi_{TT}$ . [40, 41] To estimate the energy of  $\psi_{TT}$ , they assume the triplet-triplet coupling energies in  $\psi_{TT}$  is small such that the energy of  $\psi_{TT}$  is equal to the energy of two triplet excitons each sitting on one molecule; therefore,  $E(\psi_{TT}) = 2E(\psi_T)$ . As a result, they proposed that for a system which exhibits efficient SF, the energy of the singlet must be higher than the twice of the energy of the triplet ( that is  $E(\psi_{FE}) \geq 2E(\psi_T)$  ).

Hence, Ratner and coworkers study the energy gap by applying time dependent density functional theory (TD-DFT) calculations. They find a correlation between the energy gap and the sum of transfer integrals including the transfer integrals between HOMO and HOMO as well as LUMO and LUMO. Their results provide a way to design materials with higher SF efficiency. They emphasize that the energy matching between the lowest singlet and triplet excited state ( that is  $E(\psi_{FE}) \geq 2E(\psi_T)$  ); however, their focus on the energy gap may not be sufficient to fully explain the SF efficiency because large intermolecular couplings are also vital conditions for high singlet fission efficiency. Also, their work does

not explain the mechanism of SF.

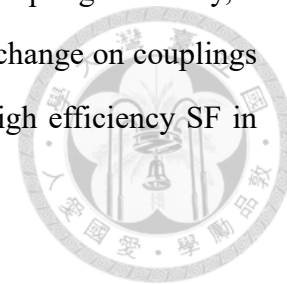
The weak direct coupling obtained by TD-DFT calculation supports the exclusion of the direct mechanism and emphasize the importance of the  $\psi_{CT}$  involvement. [42] The validity of direct mechanism and  $\psi_{CT}$ -mediated mechanism were also investigated by using open quantum system theory, [42–44] and the ultrafast SF is confirmed to take place through a  $\psi_{CT}$ -mediated mechanism. Moreover, recent results suggest a significant interplay between Frenkel exciton state  $\psi_{FE}$  and correlated triplet states  $\psi_{TT}$  through the charge transfer state  $\psi_{CT}$  in acene derivatives [3, 42, 45–50]. From these results, the mechanism of the SF process is well accepted that SF is a  $\psi_{CT}$ -mediated mechanism. In other words, the mediate couplings,  $\langle\psi_{FE}|H|\psi_{CT}\rangle$  and  $\langle\psi_{CT}|H|\psi_{TT}\rangle$ , must play important roles to achieve high efficiency SF.

The mediate couplings are usually obtained from experimental data, or only restricted to the configuration interaction single (CIS) level which considers all states in single-configuration basis. [42, 44, 50, 51] For  $\psi_{TT}$  is mainly dominated by the double excited configurations, CIS calculations are not sufficient to describe the energy of  $\psi_{TT}$  and the couplings between  $\psi_{TT}$  and other excited states.

On the other hand, it is difficult if not impossible to determine the intermolecular electronic coupling directly using density functional theory (DFT) because molecular or Kohn Sham orbitals are delocalized over the entire system. Hence, multistate density functional theory (MSDFT) describes the exciton and charge-transfer wave functions of each monomer are localized within the molecular fragment, to quantify the electronic couplings between,  $\psi_{FE}$ ,  $\psi_{CT}$  and  $\psi_{TT}$ . [20] While constrained density functional theory configuration interaction (CDFT-CI) was also adopted to deal with the couplings. [52] In CDFT-CI calculations, the CI matrix is constructed, where the CSFs in the CI matrix are generated from CDFT and the diabatic state energies as well as the couplings were obtained from the block-diagonalization of the CI matrix.

However, most DFT calculations on SF so far are based on four-electron-four-orbital model, which might be qualitatively correct but not quantitatively. Plus, although DFT calculations usually require low computational cost, DFT calculations are still impossible

to directly investigate the dependence of the structural change on couplings. Clearly, a simple method for the investigation of the dependence of structural change on couplings in SF systems is highly desirable to obtain optimal geometry for high efficiency SF in organic materials.



## 1.4 Outlook

From the discussion above, it is evident that the detailed analysis of the electronic couplings considering configuration interactions and the investigation of the excited-state characters in SF are still lacking. Also, in addition to single excited configurations, double excited configurations in a larger active space beyond the minimal HOMO/LUMO model in polyacene dimers has not been systematically examined before. Therefore, we aim to investigate the effects of active space of the configuration interaction originating from double excitations.

In addition, we aim to derive a simple method in several dimer systems to evaluate relative magnitude of couplings in different geometries and maximize the SF coupling by molecular packing. This method will be useful for molecular designs with high SF efficiency, and a detailed understanding of the validity of the method could provide useful insights into the key factors controlling the behaviors of couplings in different geometry.





## Chapter 2

# Effective Singlet fission Hamiltonians from RAS-SD-EOM Calculations

### 2.1 Properties of Electronic States in SF

In this work, we consider a dimer system consisting of two molecules (labeled as molecule A and molecule B, respectively). The key spin-adapted configuration state functions (CSFs) relevant for the SF problem in a four-electron-four-orbital model are given in Fig 2.1. These configurations are spin adapted following Szabo's convention, [53] which are the eigenfunction of electronic hamiltonian,  $H$ , and the  $S_z$  operator. Note that all CSFs are denoted by  $|ket\rangle$  notation in all our works.

These spin-adapted configurations ( $|FE_A\rangle$  ( $|FE_B\rangle$ ),  $|CT_A\rangle$  ( $|CT_B\rangle$ ),  $|TT\rangle$  and  $|S_1S_1\rangle$ ) dominate the lowest lying electronic states ( $\psi_{FE}$ ,  $\psi_{CT}$ ,  $\psi_{TT}$ ), respectively which are also shown in previous studies [41]. In the figure, the blue/red color represents the localized MOs of monomer A/B, and the lower/upper line represents the HOMO/LUMO. Also, the direction of the arrows reflect the spin of the electrons.  $|FE_A\rangle$  ( $|FE_B\rangle$ ) describes the HOMO-LUMO transition localized on molecule A (B).  $|CT_A\rangle$  ( $|CT_B\rangle$ ) describes the HOMO-LUMO transition where an electron is excited from molecule A (B) to molecule B (A).  $|TT\rangle$  and  $|S_1S_1\rangle$  are double excited configurations.

Note that, these key configurations are utilized to represent the properties of  $\psi_{FE}$ ,  $\psi_{CT}$

$$\begin{aligned}
|FE_A\rangle &= \frac{1}{\sqrt{2}} \left( \begin{array}{c} \downarrow \\ \uparrow \\ \hline \end{array} \begin{array}{c} \downarrow \\ \uparrow \\ \hline \end{array} + \begin{array}{c} \uparrow \\ \downarrow \\ \hline \end{array} \begin{array}{c} \downarrow \\ \uparrow \\ \hline \end{array} \right) \\
|FE_B\rangle &= \frac{1}{\sqrt{2}} \left( \begin{array}{c} \downarrow \\ \uparrow \\ \hline \end{array} \begin{array}{c} \downarrow \\ \uparrow \\ \hline \end{array} + \begin{array}{c} \downarrow \\ \uparrow \\ \hline \end{array} \begin{array}{c} \downarrow \\ \uparrow \\ \hline \end{array} \right) \\
|CT_A\rangle &= \frac{1}{\sqrt{2}} \left( \begin{array}{c} \downarrow \\ \uparrow \\ \hline \end{array} \begin{array}{c} \downarrow \\ \uparrow \\ \hline \end{array} + \begin{array}{c} \downarrow \\ \uparrow \\ \hline \end{array} \begin{array}{c} \downarrow \\ \uparrow \\ \hline \end{array} \right) \\
|CT_B\rangle &= \frac{1}{\sqrt{2}} \left( \begin{array}{c} \downarrow \\ \uparrow \\ \hline \end{array} \begin{array}{c} \downarrow \\ \uparrow \\ \hline \end{array} + \begin{array}{c} \downarrow \\ \uparrow \\ \hline \end{array} \begin{array}{c} \downarrow \\ \uparrow \\ \hline \end{array} \right) \\
|TT\rangle &= \frac{1}{2} \left( \begin{array}{c} \uparrow \\ \downarrow \\ \hline \end{array} \begin{array}{c} \downarrow \\ \uparrow \\ \hline \end{array} + \begin{array}{c} \downarrow \\ \uparrow \\ \hline \end{array} \begin{array}{c} \uparrow \\ \downarrow \\ \hline \end{array} + \begin{array}{c} \uparrow \\ \downarrow \\ \hline \end{array} \begin{array}{c} \downarrow \\ \uparrow \\ \hline \end{array} + \begin{array}{c} \downarrow \\ \uparrow \\ \hline \end{array} \begin{array}{c} \uparrow \\ \downarrow \\ \hline \end{array} \right) \\
|S_1S_1\rangle &= \frac{1}{\sqrt{12}} \left( 2 \begin{array}{c} \uparrow \\ \downarrow \\ \hline \end{array} \begin{array}{c} \uparrow \\ \downarrow \\ \hline \end{array} + 2 \begin{array}{c} \downarrow \\ \uparrow \\ \hline \end{array} \begin{array}{c} \downarrow \\ \uparrow \\ \hline \end{array} - \begin{array}{c} \downarrow \\ \uparrow \\ \hline \end{array} \begin{array}{c} \uparrow \\ \downarrow \\ \hline \end{array} + \begin{array}{c} \uparrow \\ \downarrow \\ \hline \end{array} \begin{array}{c} \downarrow \\ \uparrow \\ \hline \end{array} + \begin{array}{c} \downarrow \\ \uparrow \\ \hline \end{array} \begin{array}{c} \uparrow \\ \downarrow \\ \hline \end{array} - \begin{array}{c} \uparrow \\ \downarrow \\ \hline \end{array} \begin{array}{c} \downarrow \\ \uparrow \\ \hline \end{array} \right)
\end{aligned}$$

Figure 2.1: Spin adapted configurations relevant to the singlet fission process problems. Red and blue are used to denote MOs belong to molecule A and B, respectively.

and  $\psi_{TT}$ . However, MOs derived from the HF calculations in a dimer system are usually delocalized, particularly in a symmetric dimer system. As a result, delocalized MOs lose the electronic structure which is important in the interpretation of excited state properties.

## 2.2 Localization of Molecular Orbitals

To properly describe the properties of these configurations, we aim to extremize the orbital populations on either molecule A or molecule B. Hence, all CSFs are described by these localized orbitals.

The method proposed by Ishikawa is adopted to obtain localized orbitals. [54] These localized MOs are obtained by doing an unitary transformation on MOs derived from Hartree-Fock (HF) method. And the unitary transformation is generated from the diago-

nalization of the overlap matrix  $\mathbf{S}$  over the atoms of molecule A.  $\mathbf{S}$  is given by

$$S_{ij} = \sum_{\mu=1}^N \sum_{\nu=1}^N C_{\mu}^i * C_{\nu}^j \langle \chi_{\mu} | \chi_{\nu} \rangle, \quad (2.1)$$

where  $i, j$  denote the HF MOs and  $\chi_{\mu}, \chi_{\nu}$  denote atomic orbitals (AOs). The system has  $2N$  AOs, AOs 1 to  $N$  belong to the molecule A while AOs  $N+1$  to  $2N$  belong to the molecule B.

## 2.3 Restricted Active Space Single and Double Equation of Motion (RAS-SD-EOM) Method

The HF method depends on a mean-field approximation which provide a convenient way to do the self-consistent procedure. However, HF calculations usually can not properly describe the electronic states for molecules. Though, the HF calculations ensures a set of MOs that can describe the energy of the ground state ( $E_{HF}$ ), this energy is higher than the exact energy of the ground state ( $E_{exact}$ ). Also, the difference between ( $E_{HF}$ ) and ( $E_{exact}$ ) called electron correlation ( $E_{corr}$ ) reflect the failure of describing the electronically excited states.

$E_{corr}$  can be divided into two parts: the first one is the static correlation, which is derived from the wave function in the HF is a single slater determinant. The single slater determinant might be a rather poor representation of a many-electron system's state such as a system with degenerate ground states. The second one is the dynamic correlation, which is derived from the electrons in the HF calculations do not instantaneously interact with each other, as they do in reality. Hence, HF calculations are not enough to describe the electronically excited state.

To go beyond the description of HF level for electronically excited states, we need to consider interactions between configurations. Configurations interaction (CI), especially full CI, which involves in the electronic couplings contributing from other configurations, gives rather accurate descriptions to electronic eigenstates. Theoretically, with a complete



basis set, the full CI calculation considering all the configurations in the system will result in the exact wavefunctions. Unfortunately, the full CI is formidable for the most systems since the numerous configurations may complicate the interpretation of the eigenstates properties. Plus, double excited configurations are required to properly describe the property of  $\psi_{TT}$ . Hence, configuration interaction single and double (CISD) method is adopted to describe the electronic states.

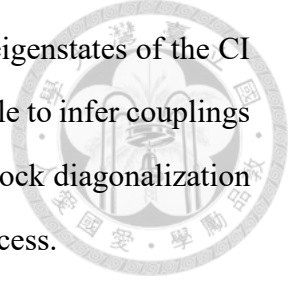
Moreover, to satisfy the size-consistent condition, the ground state configuration is neglected according to the works of David. Yaron. [55] The work done by David. Yaron describes that the energy of the electronic state should not depend on the number of the non-interacting butadiene, which forms a polyacetylene chain. However, due to size inconsistency, in CISD calculations, the energy of a single butadiene molecule is described more accurately than the energy of two or more butadiene molecules. On the other hand, the energy in different length of the polyacetylene chain calculated from SD-EOM stay consistent, which means SD-EOM calculations hold the size consistency. Hence, we follow the process of neglecting ground state configuration and using only single and double excited configurations to describe excited states.

Note that, even on a minimal basis set such as STO-3G, the full SD-EOM is still a difficult task. Since the number of CSFs determine the computational cost of the calculations, and the computational cost quickly increases with the number of active orbitals, it may be desirable to use a smaller set of CSFs. As a result, the restricted active space is used to reduce the computational cost.

Finally, the CI matrix is constructed by applying RAS-SD-EOM and the size of the CI matrix is the number of CSFs generated from the given active space. The diagonal terms of the CI matrix are the energies of the CSFs and the off-diagonal terms are the configurational couplings. For example, the active space restricted in (2,2) means that we consider all the single and double excited configurations related to the two highest occupied-localized orbitals and the two lowest unoccupied-localized orbitals in the dimer systems i.e. localized HOMO and LUMO of two molecules. Moreover, the total number of the configurations generated from (2,2) is 14. This means that the 14 by 14 CI matrix

is constructed by RAS-SD-EOM with the active space restricted in (2,2).

In general, the excited state of a system can be described by the eigenstates of the CI matrix, which are also called adiabatic states. However, it is impossible to infer couplings and dynamics in CI eigenstates. In the next section, we will apply block diagonalization to investigate the interactions between CSFs important to the SF process.



## 2.4 Three-state Model

With the aim to investigate the dynamic of SF following the Fermi's Golden rule, which describes the population transfer between the diabatic states, the CI matrix needs to be block diagonalized to transform the adiabatic CI eigenstates into the diabatic states and can get the information of electronic couplings shown in Fig. 2.2. [56]

Among the unlimited ways to divide the CI matrix into several blocks, it is rational to choose the one can give rise to the block-diagonalized states being representative of the low-lying CI eigenstates discussed i.e. has similar electronic structure. Hence, we use the p-value to divide the CI matrix into the FE block, the TT block and the CT block which represent the properties of  $\psi_{FE}$ ,  $\psi_{TT}$  and  $\psi_{CT}$ . And the p-value is defined as

$$P_{ij} = \left| \frac{\langle i|H|j\rangle}{E_i - E_j} \right|, \quad (2.2)$$

where i and j are excited configurations.  $E_i$  is the configurational energy of the i-th configuration, which is calculated from  $\langle i|H|i\rangle$ .

Note that the configurations shown in Fig. 2.1 are intuitively assigned into the three block respectively due to the properties of these configurations.  $|FE_A\rangle$  and  $|FE_B\rangle$  are assigned into FE block,  $|CT_A\rangle$  and  $|CT_B\rangle$  are assigned into CT block, and  $|TT\rangle$  and  $|S_1S_1\rangle$  are assigned to TT block. The other configurations in CI space, take configuration  $|i\rangle$  for example, we can calculate its p-value with  $|FE_A\rangle$  ( $P_{i,FE_A}$ ),  $|FE_B\rangle$  ( $P_{i,FE_B}$ ),  $|CT_A\rangle$  ( $P_{i,CT_A}$ ),  $|CT_B\rangle$  ( $P_{i,CT_B}$ ),  $|TT\rangle$  ( $P_{i,TT}$ ),  $|S_1S_1\rangle$  ( $P_{i,S_1S_1}$ ). By comparing the magnitude of  $P_{i,FE_A}$ ,  $P_{i,FE_B}$ ,  $P_{i,CT_A}$ ,  $P_{i,CT_B}$ ,  $P_{i,TT}$  and  $P_{i,S_1S_1}$ ,  $|i\rangle$  is assigned to CT block if the magnitude of either  $P_{i,CT_A}$  or  $P_{i,CT_B}$  is the largest.

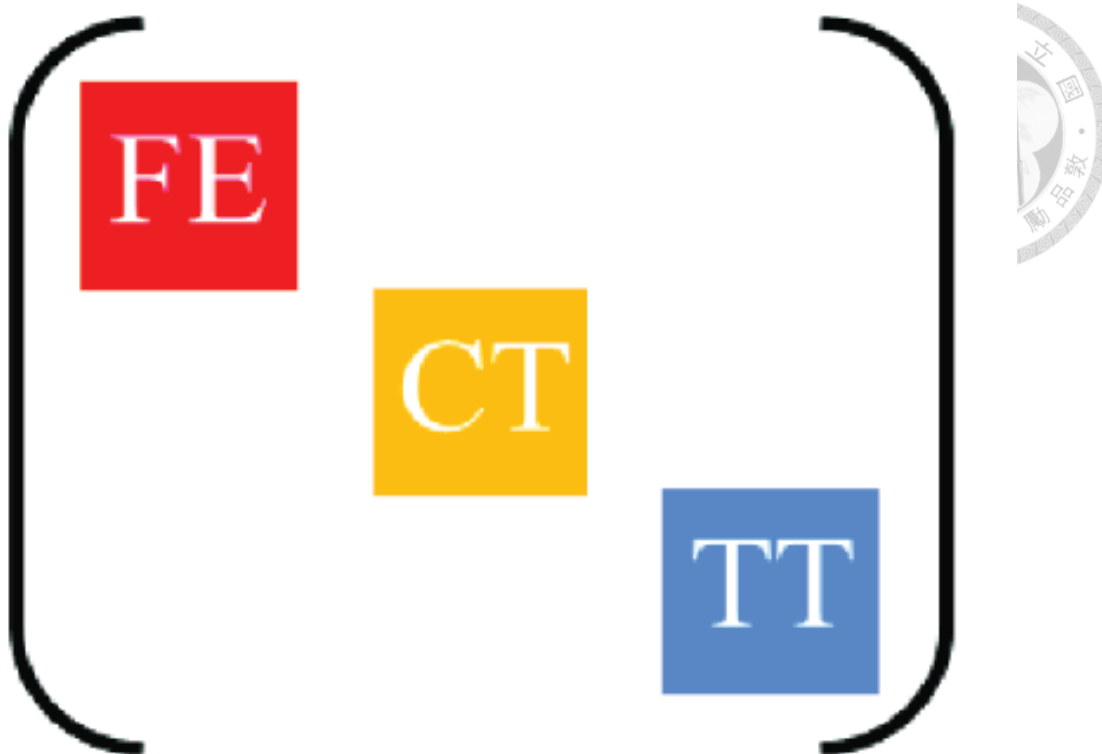


Figure 2.2: Illustration of block diagonalization of the truncated CI matrix. (FE block, CT block and the TT block)

After assigning all configurations, we do the diagonalization for three blocks, and the lowest-lying states in the three blocks are used as the basis of a three state effective hamiltonian. As a result, the diagonal terms of the effective hamiltonian represent the energy of  $\psi_{FE}$ ,  $\psi_{TT}$  and  $\psi_{CT}$ , and the off-diagonal terms are the couplings between  $\psi_{FE}$ ,  $\psi_{TT}$  and  $\psi_{CT}$ . Previous work has shown that the first singlet excited state in each block indeed has the same main features with the the lowest three CI eigenstates, which confirms that the  $\psi_{FE}$ - $\psi_{TT}$ - $\psi_{CT}$  three-state model is valid to investigate the dynamics of SF.

## 2.5 Model Dimer Systems

In this chapter, we investigate polyacene dimers in a slip-stacked geometry. To obtain atomic positions, polyacene monomers are first optimized using the DFT method with B3LYP/6-311G(++), and the structures are constrained to the  $D_{2h}$  symmetry. The optimized monomers are then aligned to a slip-stacked  $C_{2h}$  dimer structure with a faced-to-

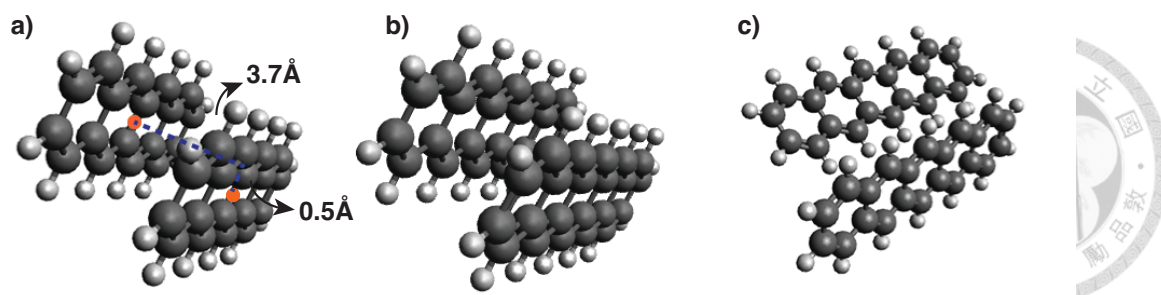


Figure 2.3: The three state model systems studied in this chapter (a) tetracene. (b) pentacene. The face-to-face distance is  $3.7\text{\AA}$  and the displacement of the slip in short axis is of  $0.5\text{\AA}$ . The nearest crystal pair of (c) pentacene.

faced distance of  $3.7\text{\AA}$  and a  $0.5\text{\AA}$  slip in the direction of the short axis shown in Fig. 2.3 (a) and (b).

The particular molecules and the slip-stacked geometry are chosen because of previous experimental results. [36–39] The previous results observe the SF in tetracene and pentacene crystals. Also, the face-to-face distance of  $3.7\text{\AA}$  is based on the geometry suggested by Zimmerman and coworkers, [36] where the conical intersection of  $\psi_{FE}$  and  $\psi_{TT}$  is located, making SF most probable to take place through internal conversion. From the geometrical effect analysis conducted by Michl and coworkers, [2] the short-axis slip ensures the nonzero value of the direct coupling due to a symmetry breaking of the MO interactions.

Considering a real system, we choose pentacene crystal to perform our calculation because the efficient SF process was observed in pentacene crystal. Note that, the calculations are not performed in the unit cell of the pentacene crystal but performed in the nearest pentacene crystalline dimer shown in Fig. 2.3 (c). [23–30]

## 2.6 Basis Set Dependence of Effective Hamiltonian in Ethylene dimer

In previous works, the minimal basis set, STO-3G, is adopted to derive MOs because the minimal basis set has the lowest computational cost and the  $\pi$  orbitals which play important roles in the conjugated systems have been already included in the minimal basis

set. However, previous studies usually use a larger basis set such as 6-31G in conjugated systems. [57–63] It is required to investigate the dependence of basis sets on the diabatic state energies and couplings.

Because the computational cost is too high to utilize a large basis set such as 6-311G to construct the SF effective hamiltonian in tetracene or pentacene dimer system, we investigate the basis set dependence in the slip-stacked ethylene dimer in which the monomer is the simplest conjugated system. In the slip-stacked ethylene dimer, there is a 0.5Å displacement along the long axis compared with the face-to-face ethylene dimer. And in all calculations, the active space of the effective hamiltonian is fixed to (2,2).

Figure 2.4(a) shows that the dependence of basis sets on the diabatic state energies. In the minimal basis set, STO-3G, the calculations overestimate  $E(\psi_{FE})$  and  $E(\psi_{CT})$  while underestimate  $E(\psi_{TT})$  such that the energy gap between  $\psi_{FE}$  and  $\psi_{TT}$  is much larger than the energy gaps in other basis sets. The dependence of basis set on the diabatic state energies shows that the minimal basis is not sufficient to construct the effective hamiltonian in conjugated systems.

On the other hand, in Fig. 2.4(b), the diabatic state couplings present a property describing that the couplings stay consistent in different basis sets. This property means that the basis sets affect little on the couplings. Note that  $\langle \psi_{FE} | H | \psi_{TT} \rangle$ , where  $H$  is the electronic hamiltonian, in STO-3G is much smaller than  $\langle \psi_{FE} | H | \psi_{TT} \rangle$  in other basis sets, but  $\langle \psi_{FE} | H | \psi_{CT} \rangle$  and  $\langle \psi_{CT} | H | \psi_{TT} \rangle$  are quite larger than  $\langle \psi_{FE} | H | \psi_{TT} \rangle$  in all basis sets. As a result, the relative small difference of  $\langle \psi_{FE} | H | \psi_{TT} \rangle$  between STO-3G and other basis sets does not affect the property.

In summary, SF hamiltonian constructed in different basis sets shows that the energy gap between  $\psi_{FE}$  and  $\psi_{TT}$  is overestimate in STO-3G and the choice of the basis sets affect little on the couplings. It is required to use a larger basis sets than STO-3G such as 6-31G to construct the effective hamiltonian while the minimal basis set is enough to describe the diabatic state couplings.

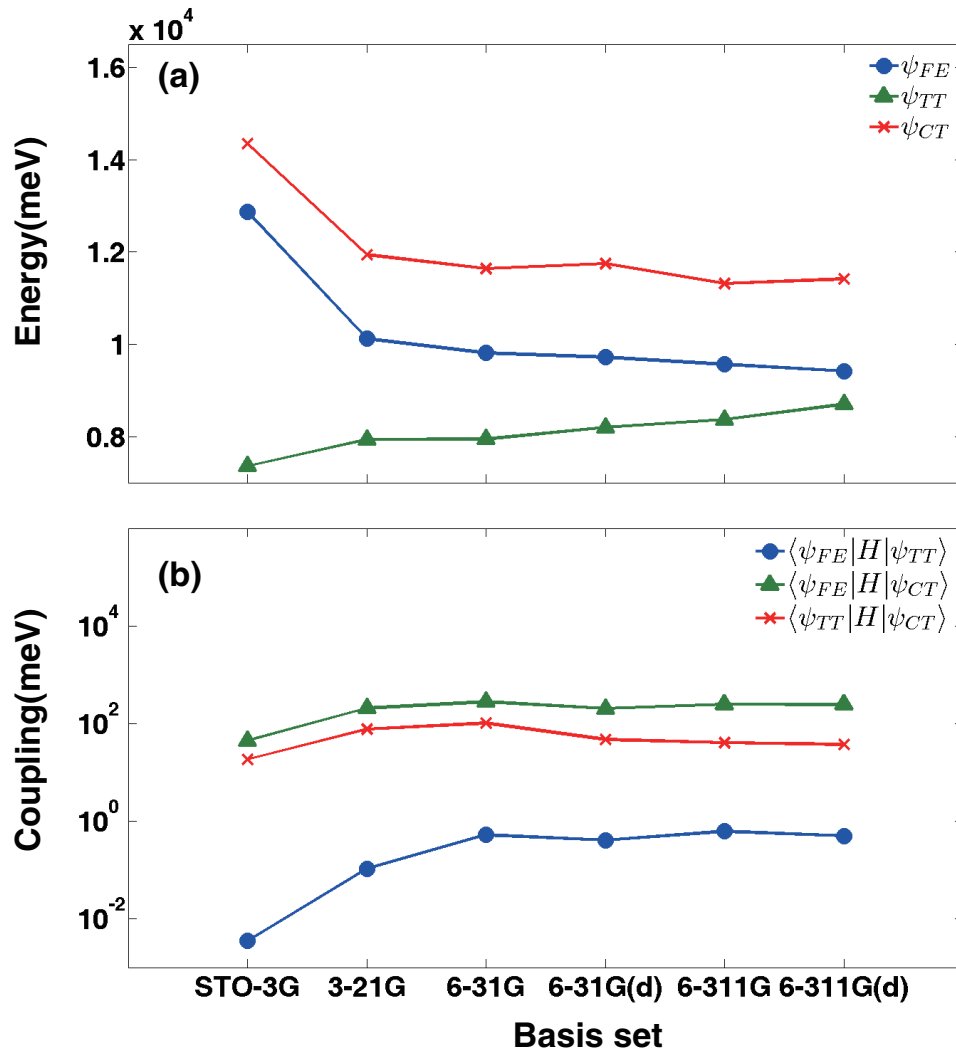
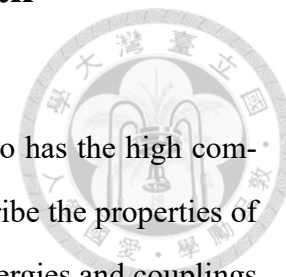


Figure 2.4: The dependence of basis set on (a) energy (b) coupling in ethylene dimer system.

## 2.7 Active Space Dependence of Hamiltonian



Although expanding to a large active space is straightforward, it also has the high computational cost. To avoid high computational cost and properly describe the properties of electronic state, we examine the convergence of the diabatic state energies and couplings in different size of the active space. Start with using the minimal active space, (2,2), to construct the SF effective hamiltonian containing 14 configurations, and expand the active space to (10,10) to construct the effective hamiltonian containing 5150 configurations.

We expect the effective SF hamiltonians can reflect the properties in tetracene and pentacene dimer systems. From the previous results of tetracene and pentacene, [36–39] the relationship between diabatic state energies in tetracene is  $E(\psi_{CT}) > E(\psi_{TT}) > E(\psi_{FE})$  while in pentacene, the relationship is  $E(\psi_{CT}) > E(\psi_{FE}) > E(\psi_{TT})$ . Also, the SF process is a mediated mechanism, which indicates that  $\langle \psi_{FE} | H | \psi_{CT} \rangle$  and  $\langle \psi_{CT} | H | \psi_{TT} \rangle$  are large while  $\langle \psi_{FE} | H | \psi_{TT} \rangle$  should be close to zero.

Figure 2.5 shows that the diabatic state energies in the different size of active space. The diabatic state energies decrease as the active space expands because that there are more excited configurations coupled with the diabatic states as the active space is bigger. However, the relationship of the energy between two diabatic state changes as the active space expands and this result can not reflect the property of the diabatic state energy like previous results in tetracene and pentacene. [36–39]

The results do not present a consistent relationship between diabatic state energies. For example, in tetracene model system, Fig. 2.5(a) shows that the relationship between  $E(\psi_{TT})$  and  $E(\psi_{CT})$  reverses from (6,6) to (8,8). This is because some excited configurations which are included when we expand the active space from (6,6) to (8,8) have strong couplings with  $\psi_{TT}$ . Moreover, another reverse of relationship between  $E(\psi_{TT})$  and  $E(\psi_{CT})$  is also observed from (8,8) to (10,10). When we expand the active space from (8,8) to (10,10), some excited configurations strongly couple to  $\psi_{CT}$ ; hence, the  $E(\psi_{CT})$  is lower than  $E(\psi_{TT})$  again.

Even the effective hamiltonian ( $\psi_{FE}$ ,  $\psi_{CT}$ ,  $\psi_{TT}$ ) in (10,10),

$$H_{tetracene} = \begin{bmatrix} 3027 & 289 & 3.2 \\ 289 & 3449 & 29.7 \\ 3.2 & 29.7 & 3617 \end{bmatrix},$$



which contain the most number of CSFs in our calculations can not explain the experimental results in tetracene.  $E(\psi_{CT})$  is 3449 meV while  $E(\psi_{TT})$  is 3617 meV, which contradicts the experimental results describing  $E(\psi_{TT}) < E(\psi_{CT})$ . [39]

In the other two systems, pentacene model system and the crystalline dimer, we can also observe the reverse of relationship between diabatic state energies from (4,4) to (6,6). Similarly the effective hamiltonians ( $\psi_{FE}$ ,  $\psi_{CT}$ ,  $\psi_{TT}$ ) of these two systems in (10,10),

$$H_{pentacene} = \begin{bmatrix} 2507 & 436 & 10.0 \\ 436 & 2670 & 43.4 \\ 10.0 & 43.4 & 2733 \end{bmatrix}$$

and

$$H_{pentacene\ crystal} = \begin{bmatrix} 2989 & 68.4 & 0.1 \\ 68.4 & 3421 & 76.0 \\ 0.1 & 76.0 & 3360 \end{bmatrix},$$

where the unit is meV, also can not reveal the special property of diabatic state energy like the previous results which describes that  $E(\psi_{TT}) < E(\psi_{FE})$ . [36–38]

In addition, the relationship of energy between states in tetracene and pyrene are quite different. Though the both systems are similar. Compare Fig. 2.5(a) with Fig. 2.5(b),  $E(\psi_{FE})$  is much smaller than  $E(\psi_{CT})$  and  $E(\psi_{TT})$  in tetracene, while  $E(\psi_{FE})$ ,  $E(\psi_{CT})$  and  $E(\psi_{TT})$  are close to each other in the both pentacene dimer systems. This indicates that molecules that also belong to polyacenes, such as atracene and hexacene, may present totally different relationship of energy from tetracene and pentacene.

The SF effective hamiltonians in these three systems show that the diabatic state energies are strongly affected by the size of the active space, which means that the multi-



configurational effect is important. Moreover, the wrong relationship between diabatic state energies and the inconsistency of the relationships implies that double CI calculation is not enough to describe the dynamics of the SF process in a dimer system. A higher level calculation should be used to correctly derive diabatic state energies or adopt semi-empirical method to obtain energies.

On the other hand, Fig. 2.6 shows that the SF process is a mediated mechanism in the three dimer systems because the direct coupling,  $\langle\psi_{FE}|H|\psi_{TT}\rangle$ , is near zero and both  $\langle\psi_{FE}|H|\psi_{CT}\rangle$  and  $\langle\psi_{CT}|H|\psi_{TT}\rangle$  are much bigger than the direct coupling. Also, these three diabatic couplings stay consistent when the active space expands, which means that the size of the active space affects little on the couplings. Hence there should be several configurational couplings dominate the diabatic state couplings. In other words, the diabatic state couplings should be described by the couplings between key configurations i.e. HOMO-LUMO transitions.

Different from the comparison of the relationship of energy between tetracene and pentacene, Fig. 2.6(a) and (b) reveals that the diabatic state couplings in both tetracene and pentacene model dimer are similar that is  $\langle\psi_{FE}|H|\psi_{CT}\rangle > \langle\psi_{CT}|H|\psi_{TT}\rangle > \langle\psi_{FE}|H|\psi_{TT}\rangle$ . This implies the magnitude of these couplings should be similar in other polyacene dimer systems such as anthracene and hexacene.

On the other hand, when comparing Fig. 2.6(b) with 2.6(c),  $\langle\psi_{FE}|H|\psi_{CT}\rangle$  is quite different in these two systems.  $\langle\psi_{FE}|H|\psi_{CT}\rangle$  is around 450 meV in pentacene model dimer, while  $\langle\psi_{FE}|H|\psi_{CT}\rangle$  is only around 60 meV. The results indicate that  $\langle\psi_{FE}|H|\psi_{CT}\rangle$  is very sensitive to the structure of the dimer or the intermolecular distance.

## 2.8 Energy Correction by Second Order Perturbation Theory

In the previous section, we have shown that the relationship between the diabatic state energies does not stay consistent as expanding the active space from (2,2) to (10,10). Even the effective hamiltonian with active space (10,10) can not reflect the same properties with

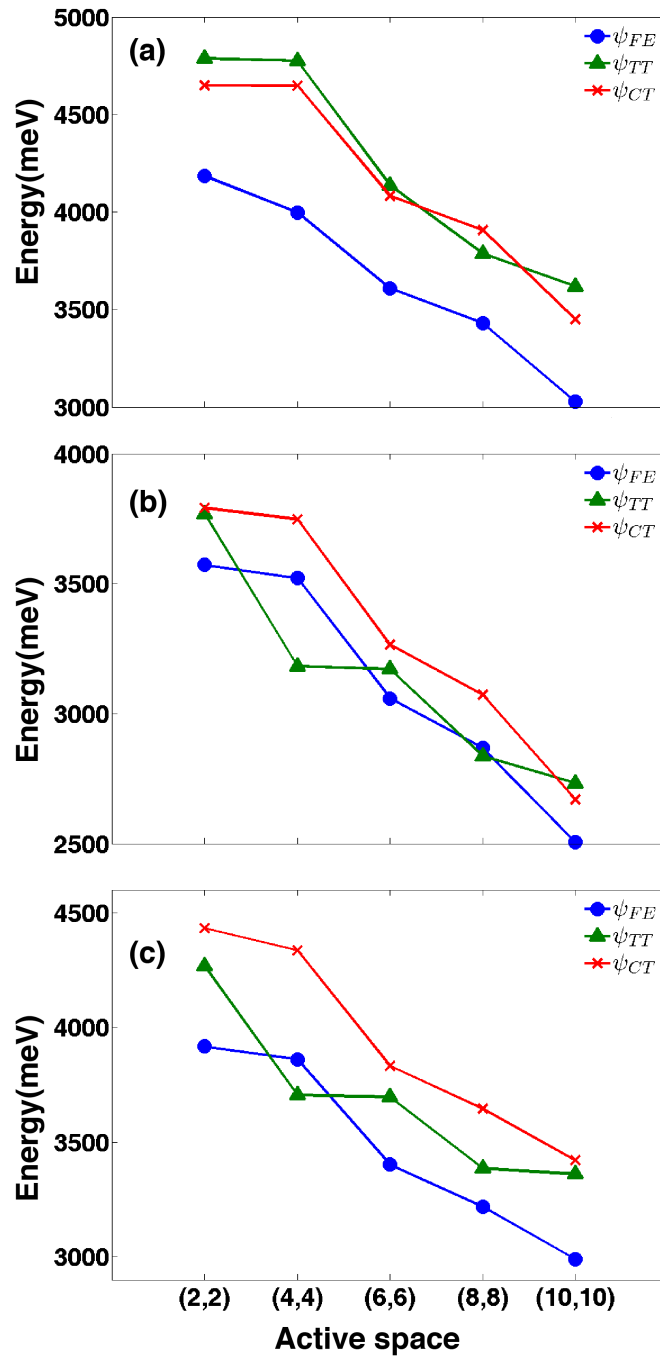


Figure 2.5: The comparison of diabatic state energy of the effective hamiltonain which is constructed in different size of active space (a) tetracene model dimer (b) pentacene model dimer (c) pentacene crystalline dimer.

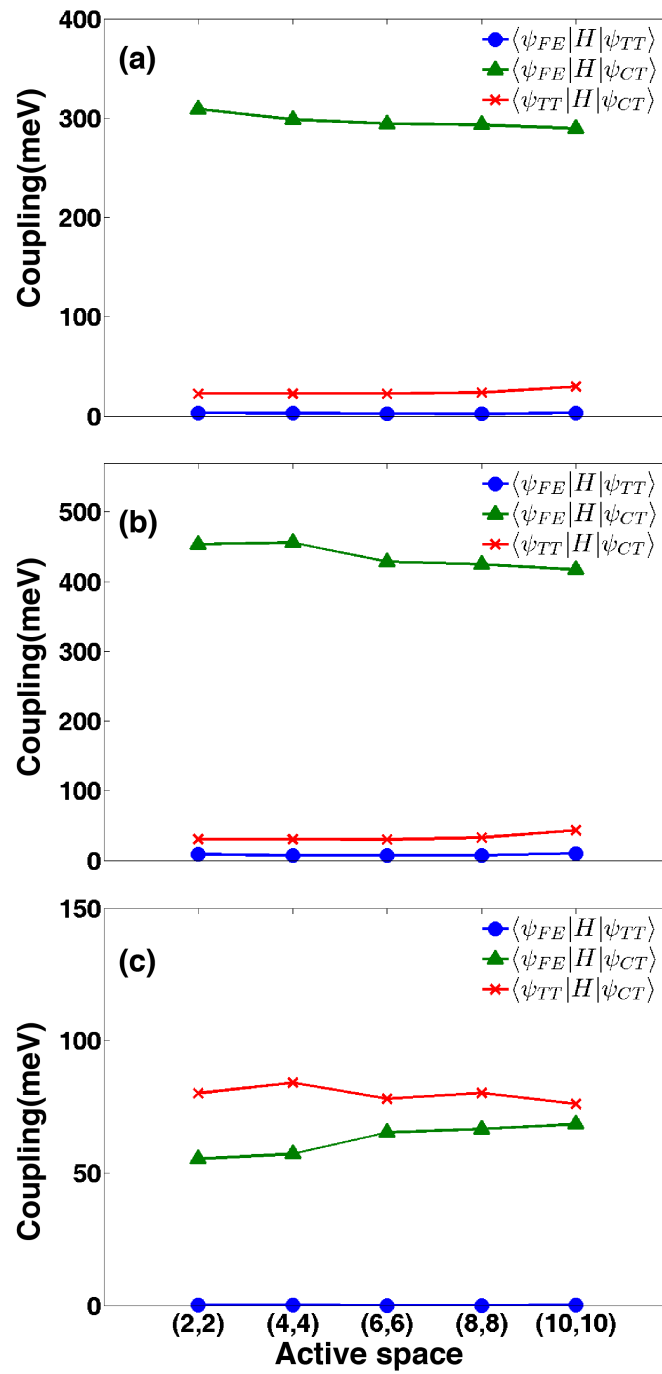


Figure 2.6: The comparison of couplings of the effective hamiltonain which is constructed in different size of active space (a) tetracene model dimer (b) pentacene model dimer (c) pentacene crystalline dimer.

the experimental results in tetracene and pentacene. This failure indicates that the diabatic state energies dismisses some important correlations, which are required to include in other ways.

For the general problems of the CI calculation, it does not consider the size consistency and the dynamic correlation. Despite the fact that SD-EOM maintains the size consistency by neglecting the ground state wavefunction, it still misses the dynamic correlation, which we believe is important in the polyacene dimer systems.

Because RAS-SD-EOM include only a little dynamic correlation while overemphasize the static correlation, striking the balance between the dynamic and static correlation in the construction of effective hamiltonian should be important. To strike the balance, the second order perturbation theory is introduced to include dynamic correlations in the diabatic state energies of the three dimer systems, which is similar to CASPT2 calculations. [64–66]

The following process presents how we introduce the second order perturbation theory to the effective hamiltonians. The size of the active space is fixed to (10,10) and the three-state effective hamiltonian is constructed by the active space that is smaller than (10,10). The other configurations that exclude the configurations contained in the three-state effective hamiltonian are regarded as the first order perturbation wavefunctions. These first order perturbation wavefunctions are utilized to generate the second-order perturbation energy. For example, if we use the minimal active space, (2,2), to construct the three-state effective hamiltonian then the 5136 configurations which exclude the configurations generated from (2,2) are considered as the first order perturbation wavefunctions to correct the diagonal terms of the effective hamiltonian.

Figure 2.7 shows that the diabatic state energies are corrected by second order perturbation theory in different size of active space. Note that when the active space is expanded to (10,10), the effective hamiltonian is equal to the results shown in the previous section, in other words, the effective hamiltonian does not corrected by the second order perturbation theory. The inclusion of the static and dynamic correlations can be controlled by manipulating the size of the active space. As we use a smaller active space to construct the

effective hamiltonian, the static correlation which is included in the effective hamiltonian also decrease, while the included dynamic correlation will increase.

The new hamiltonians in (2,2) successfully reveal the properties in tetracene and pentacene described in the previous section. In tetracene model dimer system, the new three-state effective hamiltonian ( $\psi_{FE}$ ,  $\psi_{CT}$ ,  $\psi_{TT}$ ) constructed by the minimal active space,

$$H_{tetracene} = \begin{bmatrix} 3107 & 289 & 3.2 \\ 289 & 3530 & 29.7 \\ 3.2 & 29.7 & 3239 \end{bmatrix},$$

represent consistent results compared with the experiment, which reveals that  $E(\psi_{TT}) > E(\psi_{FE})$ . [39] The new effective hamiltonians ( $\psi_{FE}$ ,  $\psi_{CT}$ ,  $\psi_{TT}$ ) in (2,2) of either the pentacene model system or the pentacene crystalline dimer system,

$$H_{pentacene} = \begin{bmatrix} 2572 & 436 & 10.0 \\ 436 & 2713 & 43.4 \\ 10.0 & 43.4 & 2132 \end{bmatrix}$$

and

$$H_{pentacene\ crystal} = \begin{bmatrix} 3073 & 68.4 & 0.1 \\ 68.4 & 3467 & 76.0 \\ 0.1 & 76.0 & 3061 \end{bmatrix},$$

also reflect the special property of diabatic state energy like the previous results which describe that  $E(\psi_{TT}) < E(\psi_{FE})$ . [36–38]

Although the relationship of the energy between diabatic states seems to be the same with the results of the experiments, we emphasize that it is a test to perform that the balance between dynamic and static correlation is important in these systems. We believe that the effective hamiltonian including the minimal active space achieves the balance between dynamic and static correlation. Thus, it can present the same properties with the experimental results.

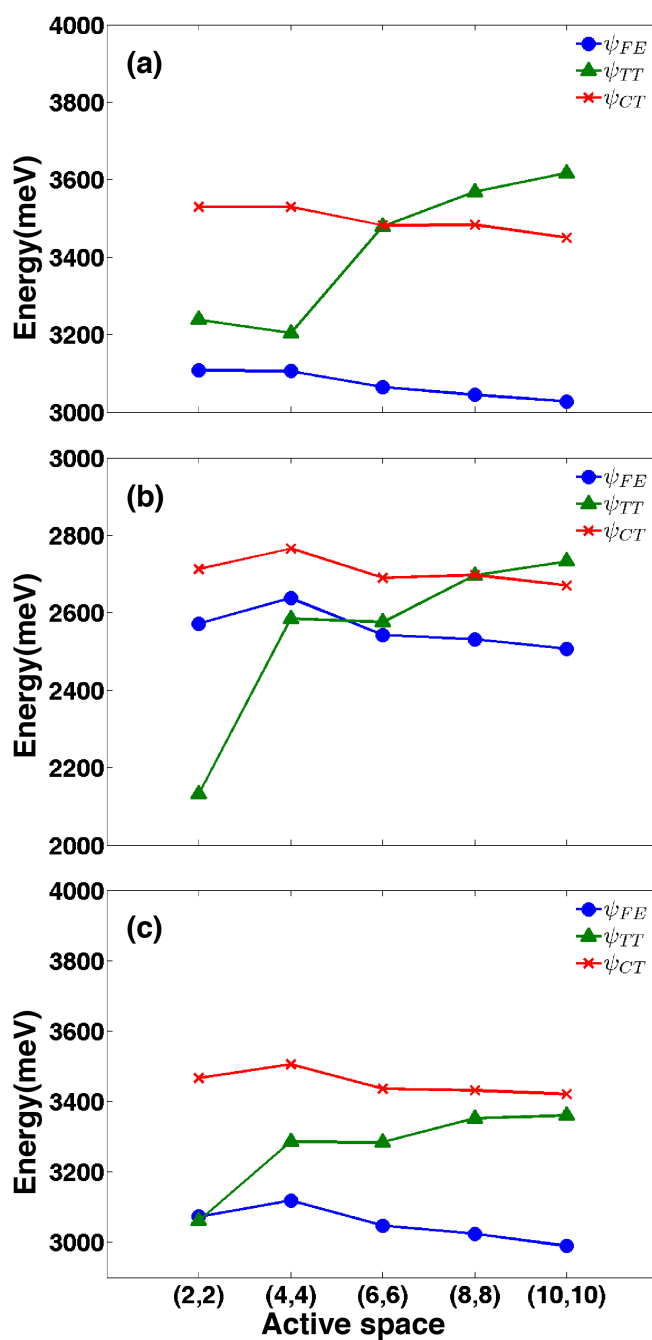
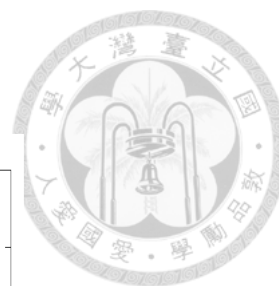


Figure 2.7: The comparison of diabatic state energy corrected by CASPT2 with different size of active space included in effective hamiltonian (a) tetracene model dimer (b)pentacene model dimer (c) pentacene crystal.





## Chapter 3

# The Dependence of Geometrical Change on Couplings

### 3.1 SF Couplings and Orbital Overlaps

In general, the SF efficiency depends on two conditions: the first one is the energy level matching which is fully described by Ratner. [40, 41] The second one is the SF couplings.

Moreover, it is expected that the SF couplings should depend critically on the geometrical changes. And the geometrical changes can be divided into two parts: the slip displacement and the relative orientation, which will be introduced later. Because of the high computational cost of CI calculations, it is hard to investigate the dependence of the geometrical change on SF couplings directly. Thus, finding a indicator which is easily calculated is required to elucidate the behaviors of SF couplings as the geometry changes. We aim to show that the key couplings can be described by the overlap integrals. These overlap integrals will be used to estimate the dependence of geometrical changes on SF couplings in dimers systems.

#### 3.1.1 Four-Electron-Four-Orbital Approximation

From the previous chapter, we have shown that the SF electronic couplings are affected little by the choice of the basis sets and the size of the active space. Hence, the diabatic



state couplings should be dominated by key configurational couplings. And these key configurations are HOMO-LUMO transitions, including  $|FE\rangle$ ,  $|TT\rangle$  and  $|CT\rangle$ .

Practically, two monomers have some interactions with each other; therefore,  $|FE\rangle$  we really concern is the linear combination of  $|FE_A\rangle$  and  $|FE_B\rangle$  as given in fig 2.1. For the same reason,  $|CT\rangle$  is the linear combination of  $|CT_A\rangle$  and  $|CT_B\rangle$ . For example,  $|FE\rangle = 1/\sqrt{2}|FE_A\rangle + 1/\sqrt{2}|FE_B\rangle$  and  $|CT\rangle = 1/\sqrt{2}|CT_A\rangle + 1/\sqrt{2}|CT_B\rangle$  are considered in a symmetric dimer system. And these key configurations ( $|FE\rangle$ ,  $|TT\rangle$  and  $|S_1S_1\rangle$ ,  $|CT\rangle$ ) dominant the lowest lying diabatic states ( $\psi_{FE}$ ,  $\psi_{TT}$ ,  $\psi_{CT}$ ), respectively, which are also shown in previous studies [41]. Thus, the previous results and our works allow us to apply four-electron-four-orbital model based on HOMO and LUMO of the monomers to describing the key characters of the diabatic states.

In this case, diabatic state couplings,  $\langle\psi_{FE}|H|\psi_{CT}\rangle$  and  $\langle\psi_{TT}|H|\psi_{CT}\rangle$ , can be approximated as  $\langle FE|H|CT\rangle$  and  $\langle TT|H|CT\rangle$ ,  $\langle S_1S_1|H|CT\rangle$  respectively. These couplings are given by

$$\langle\psi_{FE}|H|\psi_{CT}\rangle \simeq \langle FE|H|CT\rangle, \quad (3.1)$$

and

$$\langle\psi_{TT}|H|\psi_{CT}\rangle \simeq C_1\langle TT|H|CT\rangle + C_2\langle S_1S_1|H|CT\rangle, C_1 \neq C_2, \quad (3.2)$$

where  $C_1$  and  $C_2$  are the coefficients of the configurations. Note that  $\psi_{TT}$  is a multi-excitonic state so  $\psi_{TT}$  must contain both  $|TT\rangle$  and  $|S_1S_1\rangle$  from the sight of the CI method. The ratio of these two configurations in  $\psi_{TT}$  should not be equal because the energy of  $|TT\rangle$  and  $|S_1S_1\rangle$  are different even in a symmetric dimer system, which implies that  $C_1$  and  $C_2$  are not equal. On the other hand,  $|FE\rangle$  and  $|CT\rangle$  can be expanded as  $1/\sqrt{2}|FE_A\rangle + 1/\sqrt{2}|FE_B\rangle$  and  $1/\sqrt{2}|CT_A\rangle + 1/\sqrt{2}|CT_B\rangle$  for we only consider symmetric dimer in our works such that

$$\langle FE|H|CT\rangle = \frac{1}{2}(\langle FE_A|H|CT_A\rangle + \langle FE_A|H|CT_B\rangle + \langle FE_B|H|CT_A\rangle + \langle FE_B|H|CT_B\rangle) \quad (3.3)$$

### 3.1.2 Expansion of Configurational Couplings

These configurational couplings can be rewritten into two electron integrals and off-diagonal terms of the Fock matrix  $f$  [53], given by

$$\begin{aligned}\langle FE|H|CT\rangle &= (l_A h_A | l_B h_A) + (l_A h_A | l_A h_B) + \frac{1}{2}[(h_A h_A | l_A l_B) + (h_A h_B | l_A l_A)] \\ &+ (l_B h_B | l_A h_B) + (l_B h_B | l_B h_A) + \frac{1}{2}[(h_B h_B | l_B l_A) + (h_B h_A | l_B l_B)] \\ &+ \langle l_A | f | l_B \rangle + \langle h_A | f | h_B \rangle,\end{aligned}\quad (3.4)$$

where two electron integral  $(l_A h_A | l_B h_A)$ , for example, is defined as

$$(l_A h_A | l_B h_A) = \int \int \phi_{l_A}(r_1) \phi_{h_A}(r_1) \frac{1}{r_{12}} \phi_{l_B}(r_2) \phi_{h_A}(r_2) d\tau_1 d\tau_2. \quad (3.5)$$

For all two electron integrals, A and B denotes the molecule A and molecule B.  $h$  and  $l$  denotes HOMO and LUMO. For example,  $h_A$  is the highest occupied orbitals localized on the monomer A. For a symmetric dimer,  $\langle FE_A | H | CT_A \rangle = \langle FE_B | H | CT_B \rangle$  and  $\langle FE_B | H | CT_A \rangle = \langle FE_A | H | CT_B \rangle$ , so Eq. 3.4 can be rewritten as

$$\begin{aligned}\langle FE|H|CT\rangle &= 2[(l_A h_A | l_B h_A) + (l_A h_A | l_A h_B)] + (h_A h_A | l_A l_B) \\ &+ (h_A h_B | l_A l_A) + \langle l_A | f | l_B \rangle + \langle h_A | f | h_B \rangle.\end{aligned}\quad (3.6)$$

For  $\langle TT|H|CT\rangle$  and  $\langle S_1 S_1 | H | CT \rangle$ ,  $|CT\rangle$  is also expanded and rewritten as

$$\langle TT|H|CT\rangle = \frac{1}{\sqrt{2}}(\langle TT|H|CT_A\rangle + \langle TT|H|CT_B\rangle) \quad (3.7)$$

$$\langle S_1 S_1 | H | CT \rangle = \frac{1}{\sqrt{2}}(\langle S_1 S_1 | H | CT_A \rangle + \langle S_1 S_1 | H | CT_B \rangle) \quad (3.8)$$

and both of the terms can be calculated from two electron integrals, given by

$$\begin{aligned}\langle TT|H|CT\rangle &= \frac{1}{2}[-(h_A h_A | h_B l_A) - (h_A h_B | h_A l_A) + (l_A h_B | l_B l_B) \\ &+ (h_B l_B | l_A l_B) - (h_B h_B | h_A l_B) - (h_A h_B | h_B l_B)]\end{aligned}$$

$$+(l_B h_A | l_A l_A) + (h_A l_A | l_A l_B)], \quad (3.9)$$

and

$$\begin{aligned} \langle S_1 S_1 | H | CT \rangle = & \frac{3}{\sqrt{12}} [-(h_A h_A | h_B l_A) + (h_A h_B | h_A l_A) + (l_A h_B | l_B l_B) \\ & -(h_B l_B | l_A l_B) - (h_B h_B | h_A l_B) + (h_A h_B | h_B l_B) \\ & +(l_B h_A | l_A l_A) + (h_A l_A | l_A l_B)], \end{aligned} \quad (3.10)$$

Furthermore, Eq. 3.9 and Eq. 3.10 can be contracted by symmetry such that

$$\langle TT | H | CT \rangle = -(h_A h_A | h_B l_A) - (h_A h_B | h_A l_A) + (l_A h_B | l_B l_B) + (h_B l_B | l_A l_B) \quad (3.11)$$

and

$$\langle S_1 S_1 | H | CT \rangle = \frac{6}{\sqrt{12}} [-(h_A h_A | h_B l_A) + (h_A h_B | h_A l_A) + (l_A h_B | l_B l_B) - (h_B l_B | l_A l_B)]. \quad (3.12)$$

### 3.1.3 Approximation of Two Electron Integrals

In Eq. 3.6, 3.11 and 3.12, two electron integrals contained in  $\langle FE | H | CT \rangle$ ,  $\langle TT | H | CT \rangle$  and  $\langle S_1 S_1 | H | CT \rangle$  are so-called three center two electron integrals. Three center two electron integrals can be divided into two types: coulomb exchange integral,  $(\phi_a \phi_a | \phi_b \phi_c)$ , and hybrid exchange integral,  $(\phi_a \phi_b | \phi_a \phi_c)$ .

In the coulomb exchange integral, the product of  $\phi_a$  and  $\phi_a$  is not affected by the geometry because of the same molecular orbitals. The behaviors of coulomb exchange integrals in different geometry primarily depend on the other product of  $\phi_b$  and  $\phi_c$ . For example, the behavior of  $(h_A h_A | h_B l_A)$  in different geometry is elucidated by the product of  $h_B$  and  $l_A$ . Furthermore, we claim that the product of  $h_B$  and  $l_A$  can be approximated by the overlap between the HOMO of the monomer B and the LUMO of the monomer A

i.e. HOMO-LUMO overlap. The overlap integral is given by

$$\langle I|J\rangle = \sum_{\mu} \sum_{\nu} C_{\mu}^I * C_{\nu}^J \langle \mu|\nu\rangle. \quad (3.13)$$

Since both HOMO and LUMO of the monomer are  $\pi$  orbitals, both  $\mu$  and  $\nu$  are only needed to run over all  $p_z$  orbitals. In addition, we assume the hybrid exchange integral,  $(\phi_a\phi_b|\phi_a\phi_c)$ , can also be approximated by the overlap,  $\langle \phi_b|\phi_c\rangle$ . For example,  $(h_A h_B|h_A l_A)$  will be approximated by the overlap,  $\langle h_A|l_B\rangle$ .

Hence,  $\langle \psi_{TT}|H|\psi_{CT}\rangle$  can be approximated by  $\langle h_A|l_B\rangle$  in our theory. The similar formalism can be applied to treat  $\langle \psi_{FE}|H|\psi_{CT}\rangle$ ; however, we find that the geometrical dependence mainly affects  $\langle \psi_{TT}|H|\psi_{CT}\rangle$  in our study. In addition,  $\langle \psi_{FE}|H|\psi_{CT}\rangle$  can be easily calculated from CIS because  $|\psi_{FE}\rangle$  and  $|\psi_{CT}\rangle$  are primarily dominated by single excited configurations. We aim to verify the applicability of using  $\langle h_B|l_A\rangle$  to elucidate the behavior of  $\langle \psi_{TT}|H|\psi_{CT}\rangle$  in the different slip displacement and relative orientation between two monomers.

## 3.2 Effect of Slip Displacement

In the following, we first investigate how slip displacement affects the couplings, where the slip displacement is shown in Fig. 3.1. Considering the center of the two molecules  $C_1 = (x_1, y_1, z_1)$  and  $C_2 = (x_2, y_2, z_2)$ , we define  $\Delta x = x_2 - x_1$ ,  $\Delta y = y_2 - y_1$  and  $\Delta z = z_2 - z_1$ . And the slip displacement represent the displacement either along the x-axis ( $\Delta x$ ) or the y-axis ( $\Delta y$ ).

In this section, we apply our theory to three representative model systems. We start with an ethylene dimer system for which we compare the effect of slip displacement on overlap with the effect of slip displacement on the electronic couplings calculated from the RAS-SD-EOM approach to examine the validity of using overlap as an indicator of SF couplings. The dependence of slip displacement on SF couplings in tetracene and pyrene is also studied to verify our theory further.

### 3.2.1 Ethylene

To elucidate the validity of using certain overlap integrals to estimate SF couplings, we first study the SF coupling of the ethylene dimer at different slip displacement. Ethylene is the simplest conjugated system and the simple HOMO and LUMO of the Ethylene provide convenience for us to illustrate the behavior of the overlap in different slip displacement. Figure 3.1 shows the geometry of the ethylene dimer system, where the face-to-face distance between the two ethylene molecules is fixed at 4.5Å ( $\Delta z = 4.5\text{\AA}$ ), which is determined by geometry optimization with MP2/6-31G calculation. Hereafter, all calculations are carried out using 6-31G basis set. We aim to show that effective couplings, two electron integrals, and overlap integrals relevant in the SF process have the same behaviors when the slip displacement changes.

Figure 3.2 shows that the results of the ethylene dimer system. Figure 3.2(a) shows the HOMO and LUMO of an ethylene molecule. In Fig. 3.2(b), we plot the coupling between  $|\psi_{TT}\rangle$  and  $|\psi_{CT}\rangle$  derived from the RAS-SD-EOM method,  $\langle\psi_{TT}|H|\psi_{CT}\rangle$ , as a function of the long axis (x-axis) displacement. Clearly,  $\langle\psi_{TT}|H|\psi_{CT}\rangle$ , as  $\Delta y$  is zero, exhibits a maximum at  $\Delta x = 1.5\text{\AA}$ , which is in agreement with previous calculations [5]. In addition, we also plot  $\langle TT|H|CT\rangle$  and  $\langle S_1S_1|H|CT\rangle$  as a function of  $\Delta x$ , and both of them follow the dependence of  $\Delta x$  on the diabatic coupling closely. And it indicates that couplings between the two most important CSFs in the four-electron-four-orbital model indeed dominate the diabatic couplings.

In Fig. 3.2(c), we show the dependence of  $\Delta x$  on relevant two electron integrals, which exhibits  $\Delta x$  dependence similar to  $\langle\psi_{TT}|H|\psi_{CT}\rangle$ . The behaviors of  $\langle\psi_{TT}|H|\psi_{CT}\rangle$  can be estimated by the behaviors of these two electron integrals, which are approximated by the overlap integral,  $\langle h_A|l_B\rangle$ . Figure 3.2(d) also shows that  $\langle h_A|l_B\rangle$  as a function of  $\Delta x$ , and the behavior of  $\langle h_A|l_B\rangle$  shows excellent correspondence with the behavior of  $\langle\psi_{TT}|H|\psi_{CT}\rangle$  ( Figure 3.2(b) ).

On the other hand,  $\langle\psi_{TT}|H|\psi_{CT}\rangle$  is zero when  $\Delta x$  is equal to zero regardless of the value of  $\Delta y$ , which we didn't show in the Fig. 3.2, and this phenomenon was also mentioned before [5]. Calculations of  $\langle h_A|l_B\rangle$ , which is a function of  $\Delta y$  with  $\Delta x = 0$  shows

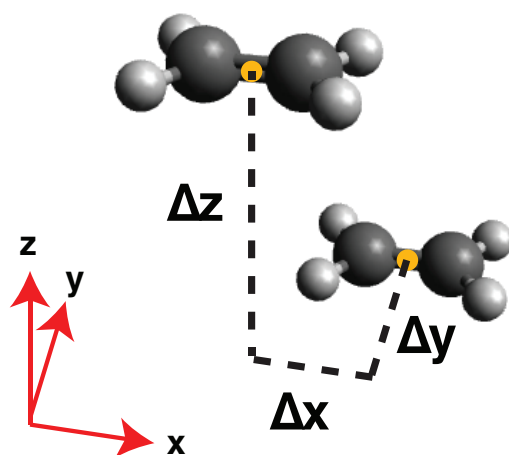


Figure 3.1: Illustration of the slip displacement, where the yellow points are the centers of the ethylene monomers.

the same behavior with  $\langle \psi_{TT} | H | \psi_{CT} \rangle$ . Apparently, in the ethylene system,  $\langle h_A | l_B \rangle$  is an excellent indicator of the dependence of the slip displacement on  $\langle \psi_{TT} | H | \psi_{CT} \rangle$ .

Besides, the dependence of the slip displacement on  $\langle h_A | l_B \rangle$  can be explained by a mirror plane. This mirror plane is perpendicular to the long axis and in the middle of the face-to-face ethylene dimer such that HOMO is symmetric while LUMO is anti-symmetric to the mirror plane. This mirror plane also explain the zero if  $\langle h_A | l_B \rangle$  in a face-to-face ethylene dimer system. Moreover,  $\langle h_A | l_B \rangle$  is zero at  $\Delta x = 0$  regardless of the value of  $\Delta y$  because the mirror plane remains in the dimer system.

In contrast, when  $\Delta y = 0$  and  $\Delta x$  become non-zero in the dimer system,  $\langle h_A | l_B \rangle$  has non-zero value since the mirror plane disappears. For a good correlation between  $\langle \psi_{TT} | H | \psi_{CT} \rangle$  and HOMO-LUMO overlap, the behavior of  $\langle \psi_{TT} | H | \psi_{CT} \rangle$  in our results can also be elucidated by this mirror plane.

The most important is that comparing Fig. 3.2(b) and (d) shows that the relative magnitude of  $\langle \psi_{TT} | H | \psi_{CT} \rangle$  can also be elucidated by  $\langle h_A | l_B \rangle$ . For example,  $\langle \psi_{TT} | H | \psi_{CT} \rangle$  as  $\Delta x = 1\text{\AA}$  is smaller than  $\langle \psi_{TT} | H | \psi_{CT} \rangle$  as  $\Delta x = 2\text{\AA}$  and  $\langle h_A | l_B \rangle$  reveals the same relationship between as  $\Delta x = 1\text{\AA}$  and as  $\Delta x = 2\text{\AA}$ . This indicates that it is possible to calculate  $\langle \psi_{TT} | H | \psi_{CT} \rangle$  from  $\langle h_A | l_B \rangle$ .

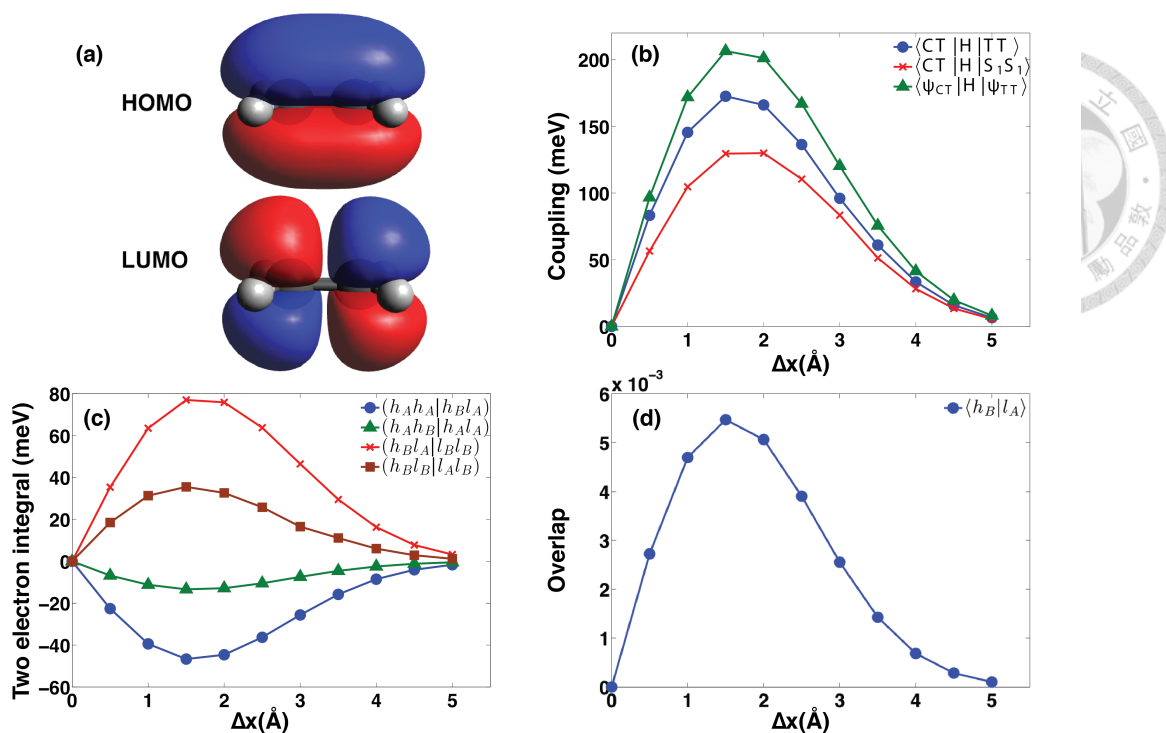


Figure 3.2: (a) Visualizations of HOMO and LUMO in ethylene monomer. The dependence of  $\Delta x$  on (b) couplings, (c) two electron integrals and (d) overlap. Other parameters are  $\Delta y = 0 \text{ \AA}$  and  $\Delta z = 4.5 \text{ \AA}$ .

### 3.2.2 Tetracene

The SF process was observed in tetracene crystals before, [9] hereafter SF process was observed in bistetracene solutions as well [31], which reveals that the structure of the dimer can be manipulated. In order to apply our theory to bistetracene for molecular design, we aim to verify that our theory can be applied to the tetracene dimer system.

Figure 3.3(a) shows the HOMO and LUMO of a tetracene molecule. In a face-to-face tetracene dimer system, there is a mirror plane perpendicular to the short axis and in the middle of the dimer system such that HOMO is anti-symmetric while LUMO is symmetric to the mirror plane. Different from the ethylene dimer system, SF couplings,  $\langle TT|H|CT \rangle$  and  $\langle S_1S_1|H|CT \rangle$ , are expected to be zero at  $\Delta y = 0$  regardless of the value of  $\Delta x$  because the mirror plane is perpendicular to the short axis and disappears only when  $\Delta y$  becomes non-zero.

Hence, we plot the couplings as a function of  $\Delta y$  (shown in Fig. 3.3(b)) to demonstrate the disappearance of the mirror plane in the tetracene dimer system. Figure 3.3(c) and (d)

show that the  $\Delta y$  dependence of relevant two electron integrals and the HOMO-LUMO overlap agree very well with the  $\Delta y$  dependence of  $\langle TT|H|CT\rangle$  and  $\langle S_1S_1|H|CT\rangle$ . Even though the patterns of HOMO and LUMO in tetracene molecule are more complicated than the patterns of orbitals in ethylene molecule, our theory still can be applied to the tetracene dimer system.

In addition, from the results of ethylene and tetracene, we can find that the direction of the mirror plane in the ethylene face-to-face dimer is different from the direction of the mirror plane in the tetracene face-to-face dimer. At the same time, in the ethylene dimers,  $\langle TT|H|CT\rangle$  and  $\langle S_1S_1|H|CT\rangle$  are zero at  $\Delta x = 0$  regardless of the value of  $\Delta y$  in the ethylene dimers, while in the tetracene dimers, the couplings are zero at  $\Delta x = 0$  regardless of the value of  $\Delta y$ . This implies that the direction of the mirror plane in the face-to-face dimer determines the appearance of the non-zero value of  $\langle TT|H|CT\rangle$  and  $\langle S_1S_1|H|CT\rangle$ , which is useful to predict the behaviors of couplings in an unknown dimer system.

In Fig. 3.3(b), the oscillatory behavior is observed.  $\langle TT|H|CT\rangle$  and  $\langle S_1S_1|H|CT\rangle$  exhibit a maximum at  $\Delta y = 3.5\text{\AA}$ , which also can be clearly illustrated by the HOMO-LUMO overlap. In Fig. 3.3(a), the mirror plane divides HOMO into two parts. When  $\Delta y$  increases, the overlap between the first part of HOMO, or the positive part, and LUMO is denoted as  $S_p$  for the overlap is always positive. While the overlap between the second part, or the negative part, and LUMO is always negative, hence  $S_n$ .

In a face-to-face tetracene dimer, where both  $\Delta x$  and  $\Delta y$  are equal to zero, the nearest distance between the positive part and the center of LUMO is equal to the nearest distance between the negative part and the center of LUMO. Hence, the absolute value of  $S_p$  and  $S_n$  are equal at  $\Delta y = 0\text{\AA}$ , which results in  $\langle h_A|l_B\rangle = 0$ .

At  $\Delta y = 3.5\text{\AA}$  with  $\Delta x$  fixed to zero, the nearest distance between the negative part and the center of LUMO become even larger so the absolute value of  $S_n$  become much smaller than  $S_n$  at  $\Delta y = 0$ . On the contrary,  $S_p$  at both  $\Delta y = 0\text{\AA}$  and  $\Delta y = 3.5\text{\AA}$  are similar because the nearest distance between the positive part and the center of LUMO at  $\Delta y = 3.5\text{\AA}$  is the same as at  $\Delta y = 0\text{\AA}$ . As a result, the HOMO-LUMO over-



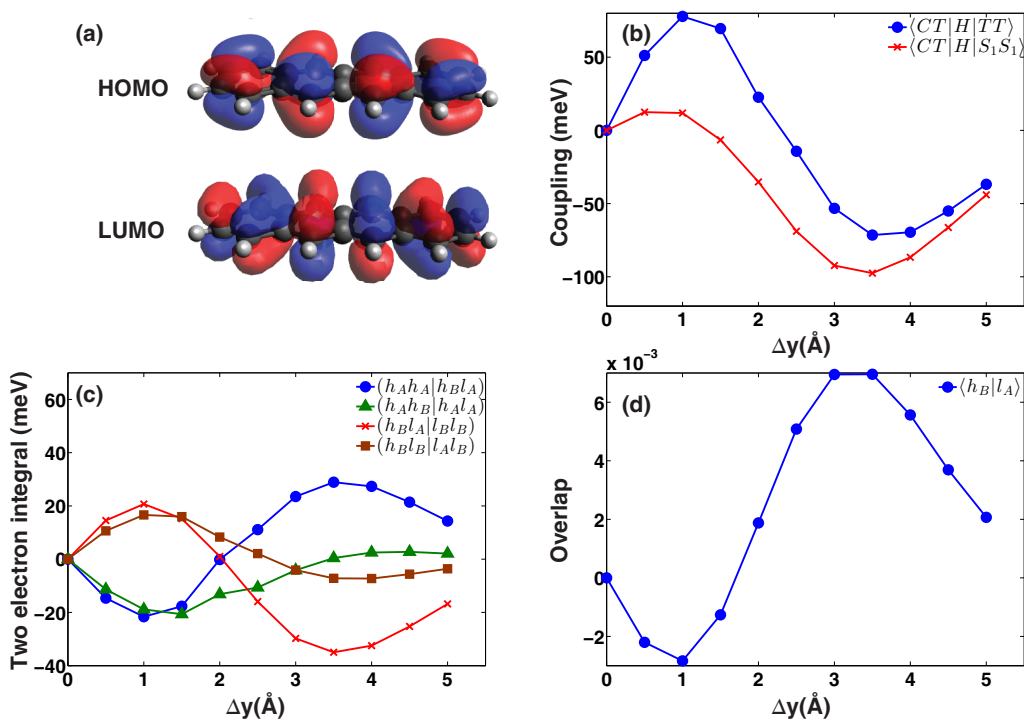


Figure 3.3: (a) Visualizations of HOMO and LUMO in tetracene monomer. The dependence of  $\Delta y$  on (b) couplings, (c) two electron integrals and (d) overlap. Other parameters are  $\Delta x = 0 \text{ \AA}$  and  $\Delta z = 4 \text{ \AA}$ .

lap ( $\langle h_B | l_A \rangle = S_p + S_n$ ) reach the maxima at  $\Delta y = 3.5 \text{ \AA}$ , which also elucidates that  $\langle TT|H|CT \rangle$  and  $\langle S_1S_1|H|CT \rangle$  reach the maxima at  $\Delta y = 3.5 \text{ \AA}$ .

Note that other polyacenes, such as anthracene and pentacene, are in the same point group as tetracene. These polyacenes should also present the same mirror plane as tetracene [67]. Although we only do the calculations in tetracene, we expect that the similar dependence of slip displacement on SF couplings in pentacene and anthracene as in tetracene.

### 3.2.3 Pyrene

The dependence of slip displacement on the SF coupling in the pyrene, another four-ring system, is also investigated because the mirror plane presented in the face-to-face pyrene dimer system is different from in the face-to-face tetracene dimer system. And the mirror plane can be determined by Fig. 3.3(a), which shows the HOMO and LUMO in a pyrene molecule.

The results in pyrene also confirm the validity of our theory. The mirror plane to which

HOMO is symmetric while LUMO is anti-symmetric is perpendicular to the long axis, and in the middle of the face-to-face pyrene dimer system. Based on our theory,  $\langle TT|H|CT\rangle$  and  $\langle S_1S_1|H|CT\rangle$  are expected to be zero at  $\Delta x = 0$  regardless of the value of  $\Delta y$ . And our results of  $\langle TT|H|CT\rangle$  and  $\langle S_1S_1|H|CT\rangle$  shown in Fig. 3.3(b), which are functions of  $\Delta x$  show the same geometric dependence with the overlap shown in Fig. 3.3(d).

A oscillatory behavior is also observed in Fig. 3.4(b) and a discrepancy is found at  $\Delta x = 3\text{\AA}$  in  $\langle S_1S_1|H|CT\rangle$ . This phenomenon results from the special behavior of  $(h_Ah_B|h_Al_A)$  as a function of  $\Delta x$ . In Fig. 3.4(c), the value of  $(h_Ah_B|h_Al_A)$  at any  $\Delta x$  is always equal to or smaller than zero. Though  $\langle h_A|l_B\rangle$  which is shown in Fig. 3.4(d) cannot fully describe  $(h_Ah_B|h_Al_A)$  as a function of  $\Delta x$ , HOMO-LUMO overlap still exhibit a similar  $\Delta x$  dependence with  $\langle TT|H|CT\rangle$  and  $\langle S_1S_1|H|CT\rangle$ . Hence, we believe that the overlap is a good indicator of the dependence of the slip displacement on the effective SF couplings in the pyrene system despite the discrepancy.

From the results in ethylene, tetracene and pyrene, we find that  $\langle TT|H|CT\rangle$  and  $\langle S_1S_1|H|CT\rangle$  are zero in all three different face-to-face dimer systems. As a result, the zero value of  $\langle TT|H|CT\rangle$  and  $\langle S_1S_1|H|CT\rangle$  must be a general property for all conjugated dimer systems. It is important because the property confirms that a face-to-face dimer can not be a good design of the SF material. The face-to-face dimer means  $\langle \psi_{TT}|H|\psi_{CT}\rangle$  must be zero in this dimer system, where SF process can not be observed.

Also,  $\langle TT|H|CT\rangle$  and  $\langle S_1S_1|H|CT\rangle$  in these three dimer systems, exhibit one or more peaks instead of a broad band as the slip displacement along the specific direction increases, which means  $\langle \psi_{TT}|H|\psi_{CT}\rangle$  is sensitive to the slip displacements. This property of  $\langle \psi_{TT}|H|\psi_{CT}\rangle$  indicates that even though two dimers' structure are similar,  $\langle \psi_{TT}|H|\psi_{CT}\rangle$  in two dimer systems may be totally different.

### 3.3 Effect of Relative Orientation

Also, the effect of the relative orientation is studied by generating the dimer systems with different relative angular position, in which one monomer is rotated about the long axis in a face-to-face dimer system. We ignore the dependence of the relative orientation about

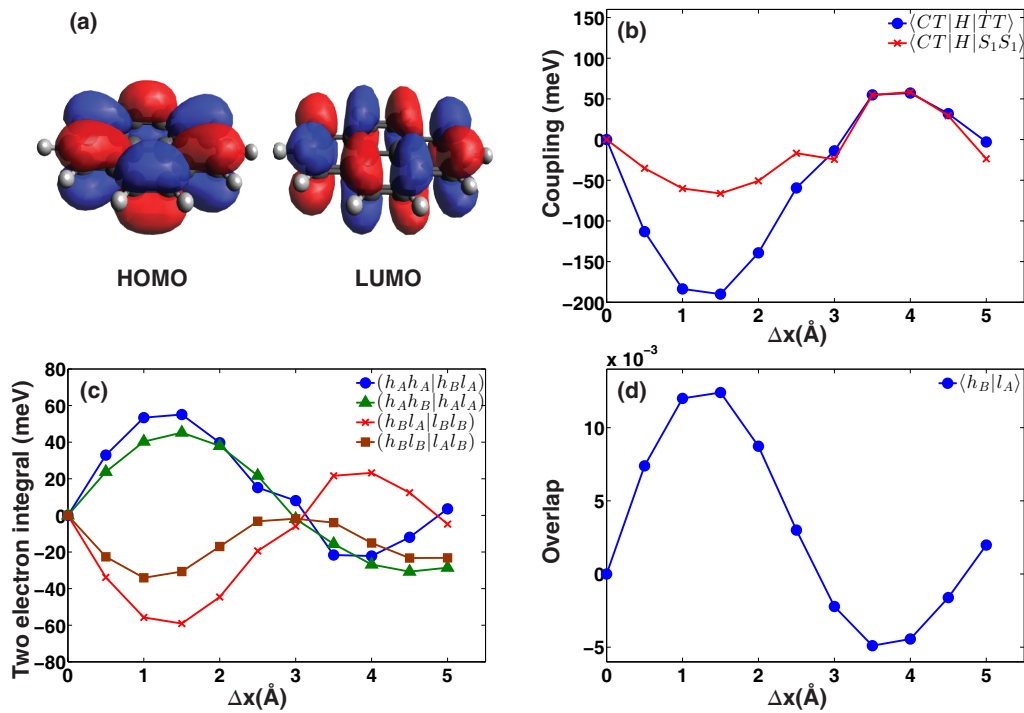


Figure 3.4: (a) Visualizations of HOMO and LUMO in pyrene monomer. The dependence of  $\Delta x$  on (b) couplings, (c) two electron integrals and (d) overlap. Other parameters are  $\Delta y = 0 \text{ \AA}$  and  $\Delta z = 4 \text{ \AA}$ .

the short axis because it is more restricted to rotate one molecular about the short axis in a dimer system. For example, in a herring bone structure, the molecule in the crystal is mainly rotated about the long axis.

We choose the tetracene dimer system to study the dependence of the intermolecular rotation on SF couplings because the SF process has been observed in tetracene crystal before [9]. Note that the  $C_2$  rotational symmetry along the x-axis in the face-to-face tetracene dimer system disappears when one molecule is rotated. As the result, the magnitude of  $\langle TT|H|CT_A \rangle$  and  $\langle TT|H|CT_B \rangle$ , for example, are not equal anymore, like in a symmetric dimer system. However, in our calculations, overlap, two electron integrals, and SF couplings are affected little by the disappearance of the  $C_2$  rotational symmetry. Hence, SF couplings are still derived by Eq. 3.9 and Eq. 3.10 just like the derivation of SF couplings in a symmetric dimer system.

Figure 3.5 shows that the rotational angle is limited to  $60^\circ$ . This is because that when the rotational angle exceeds  $60^\circ$ , two tetracene molecules are so close that two molecules are strongly correlated with each other and localized orbitals are not suitable to describe

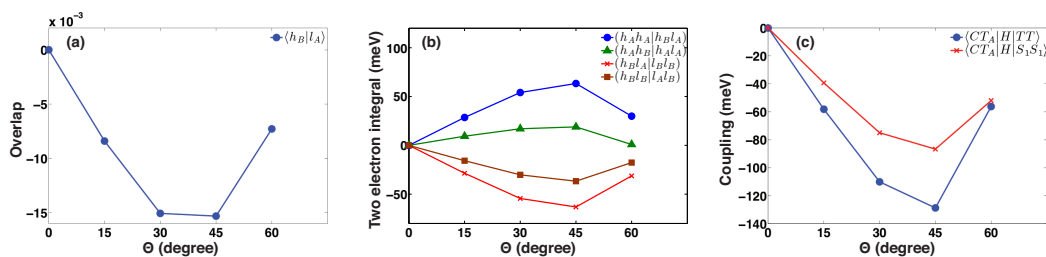


Figure 3.5: Comparisons of (a) overlap, (b) two electron integrals and (c) couplings in a face-to-face tetracene dimer with one monomer is rotated along long axis. Other parameters are  $\Delta x = 0\text{\AA}$ ,  $\Delta y = 0\text{\AA}$  and  $\Delta z = 4\text{\AA}$ .

the electronic states and the electronic couplings.

Figure 3.5 shows that the relative value of  $\langle TT|H|CT\rangle$  and  $\langle S_1S_1|H|CT\rangle$  can be illustrated by HOMO-LUMO overlap very well. Because the results show that our theory can be applied to the dimer system when one molecule of the system is rotated, we confirm that the overlap can be an indicator of the couplings when the relative orientation is changed.

Another important point is that Fig. 3.3 and Fig. 3.5 also show the possibility of calculating  $\langle TT|H|CT\rangle$  and  $\langle S_1S_1|H|CT\rangle$  from  $\langle h_A|l_B\rangle$ . The dependence of the slip displacement on both overlap and couplings are comparable with the dependence of the relative orientation on both of them. For example,  $\langle h_A|l_B\rangle$  at  $\Delta y = 1.5\text{\AA}$  and  $\Delta x = 0\text{\AA}$  is smaller than  $\langle h_A|l_B\rangle$  with the relative orientation,  $\theta$ , is  $45^\circ$ , which correspond to the comparison of  $\langle TT|H|CT\rangle$  and  $\langle S_1S_1|H|CT\rangle$  between as the slip displacement is  $\Delta y = 1.5\text{\AA}$  as well as  $\Delta x = 0\text{\AA}$ , and as the relative orientation is  $45^\circ$ .

## 3.4 Overlap as an Indicator of Couplings

### 3.4.1 2D Mapping of the Overlap Integrals

Our theory, which describes  $\langle h_A|l_B\rangle$  as a descriptor of  $\langle TT|H|CT\rangle$  and  $\langle S_1S_1|H|CT\rangle$ , successfully illustrate the behavior of  $\langle TT|H|CT\rangle$  and  $\langle S_1S_1|H|CT\rangle$  as functions of either  $\Delta x$  or  $\Delta y$ . Considering the structural change of displacements in a crystal structure, for example, one molecule has displacements along both the long axis and the short axis related to another molecule. We expect  $\langle h_B|l_A\rangle$  has large correspondence with  $\langle TT|H|CT\rangle$

and  $\langle S_1 S_1 | H | CT \rangle$  even when all of them are functions of  $\Delta x$  and  $\Delta y$ . We calculate the overlap as functions of  $\Delta x$  and  $\Delta y$  with the aim to qualitatively predict the behaviors of couplings and compare overlaps with the results of couplings. Note that all calculations in Fig. 3.6 are presented in absolute value.

Figure 3.6 shows that behaviors of the couplings depending on any given slip displacement in the xy-plane are excellently elucidated by the overlap. In Fig. 3.6(a) and (b), both of  $\langle TT | H | CT \rangle$  and  $\langle S_1 S_1 | H | CT \rangle$  in the ethylene have only one maximum, which is consistent with the works done by Michl's group [5]. Figure 3.6(d), (e), (g) and (h) show that  $\langle TT | H | CT \rangle$  and  $\langle S_1 S_1 | H | CT \rangle$  in both the tetracene and the pyrene system have more than one local maxima. This implies that there is more than one geometry which is expected to have high single fission efficiency. Also, in Fig. 3.6(c), (f) and (i), the geometries corresponding to the local maxima of overlap integrals are the same as the geometries which corresponds to the local maxima of  $\langle TT | H | CT \rangle$  and  $\langle S_1 S_1 | H | CT \rangle$  in each three systems.

Moreover, Fig. 3.6(c), (f) and (i), reveal that the distance between two centers of the molecule is not the main factor when  $\langle h_B | l_A \rangle$  is a function of  $\Delta x$  and  $\Delta y$ .  $\langle h_B | l_A \rangle$  mainly depends on the patterns of HOMO and LUMO of the monomer, which implies that the behaviors of  $\langle TT | H | CT \rangle$  and  $\langle S_1 S_1 | H | CT \rangle$  should also mainly depend on the patterns of HOMO and LUMO. In other words, if the patterns of HOMO and LUMO in two dimer systems are similar, the difference of the 2-D mapping of  $\langle TT | H | CT \rangle$  and  $\langle S_1 S_1 | H | CT \rangle$  in between two systems must be small. The maximum of the couplings appear at the similar position  $(\Delta x, \Delta y)$  in the both similar systems.

Note that, for all three systems, we did not investigate the dependence of the intermolecular distance,  $\Delta z$ , on either  $\langle h_B | l_A \rangle$  or  $\langle \psi_{TT} | H | \psi_{CT} \rangle$ . This is because that for any given atom in molecule A, the relative directions to any atom in molecule B do not change when only  $\Delta z$  increases. This indicates that the intermolecular distance is the only factor to affect  $\langle h_B | l_A \rangle$  and  $\langle \psi_{TT} | H | \psi_{CT} \rangle$  when only  $\Delta z$  increases. As a result,  $\langle h_B | l_A \rangle$  and  $\langle \psi_{TT} | H | \psi_{CT} \rangle$  simply decrease when  $\Delta z$  increases as  $\Delta x$  as well as  $\Delta y$  are fixed.

Clearly, our theory has been verified to exhibit a wide range of applications. For

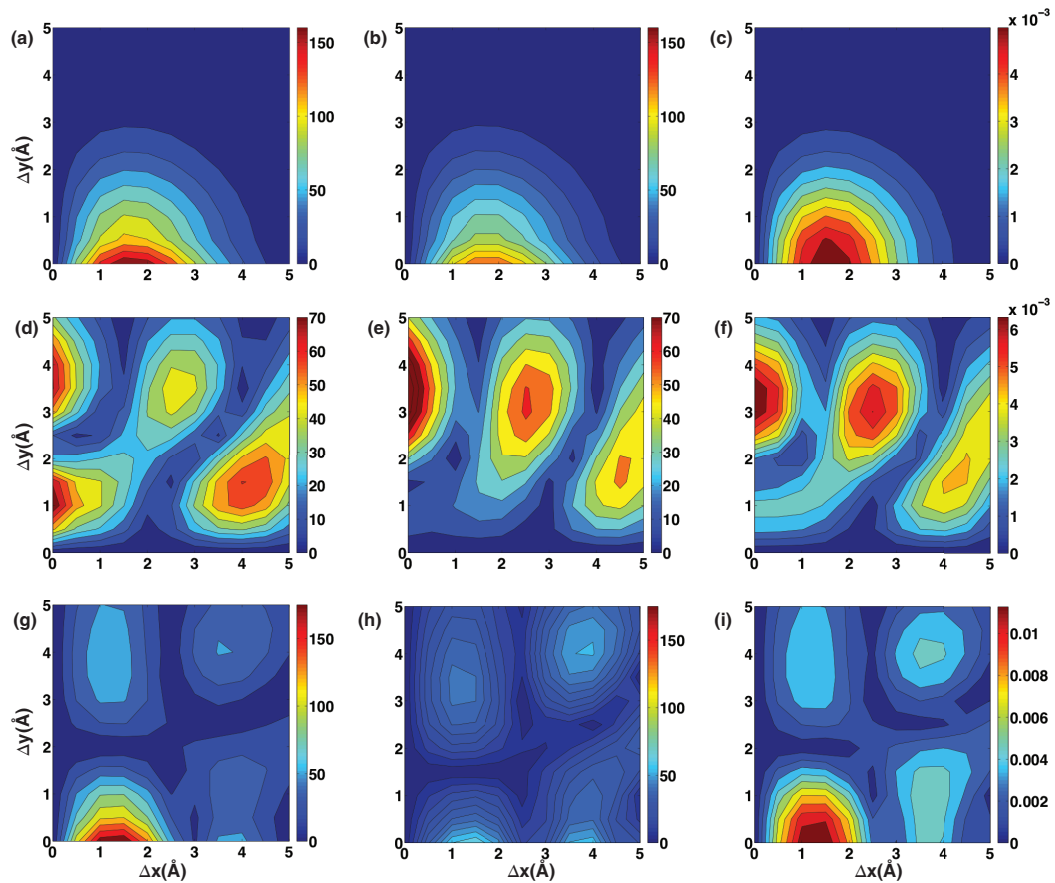


Figure 3.6: Comparisons of (a)  $\langle TT|H|CT \rangle$ , (b)  $\langle S_1 S_1|H|CT \rangle$  and (c)  $\langle h_B|l_A \rangle$ , which are functions of  $\Delta x$  and  $\Delta y$  in ethylene dimer. Accordingly, (d), (e) and (f) in tetracene as well as (g), (h) and (i) in pyrene. The units of couplings are meV.

$\langle h_B|l_A \rangle$  successfully elucidates the dependence of the geometrical change on  $\langle TT|H|CT \rangle$  and  $\langle S_1 S_1|H|CT \rangle$  in ethylene, tetracene, and pyrene, we claim that overlap can be treated as a guideline to determine an optimal geometry with largest couplings in a dimer system. This theory will be helpful for molecular design to search the optimal geometry for high SF efficiency.

### 3.4.2 Overlap in Tetracene Crystalline Pair

Because our results present that the overlap is a good indicator of the behavior of couplings when the dimer system has geometrical changes. We combine the effects of the slip displacement and the relative orientation on the overlap to predict the behaviors of SF coupling in the crystal structure, which is shown in Fig. 3.7.

Morphology and the crystal packing can play a significant role in crystal structure,

for example, tetracene crystal. [52, 68] Thus, we use the HOMO-LUMO overlap to elucidate the structural dependence of  $\langle TT|H|CT\rangle$  and  $\langle S_1S_1|H|CT\rangle$  in the nearest tetracene crystalline pair.

The overlap,  $\langle h_B|l_A\rangle$ , of the nearest tetracene crystalline pair is projected on Fig. 3.8, which shows the overlap as functions of  $\Delta y$  and  $\theta$ . The relevant  $\Delta x$  between the two molecules is neglected for  $\Delta x$  is small in tetracene crystal. In the crystalline dimer, the displacement in short axis ( $\Delta y$ ) is 0.9Å and rotational angle,  $\theta$ , is 59.4° compare with the face-to-face tetracene dimer. [69].

In Fig. 3.8, the overlap is presented in both positive and negative  $\Delta y$ . Because the  $C_2$  rotational symmetry disappear, the positive and negative  $\Delta y$  affect differently on the overlap. Besides, the black cross shows the position which corresponds to the structure of the nearest tetracene crystalline pair. We expect there is a strong coupling between the  $|\psi_{TT}\rangle$  and  $|\psi_{CT}\rangle$  in tetracene crystals because a large overlap is shown at the geometry of the nearest tetracene crystalline pair. This result also supports that singlet fission can be observed in tetracene crystal for its strong SF couplings.

Also, the maximum of  $\langle h_B|l_A\rangle$  are observed at position,  $(\Delta y, \theta)$ , equalling to (1, 60) and (-1.5, 60). Hence, the high efficiency SF process is expected to be observed in the tetracene dimer with the slip displacement,  $\Delta y = 1$  or  $-1.5\text{Å}$ , and the relative orientation,  $\theta = 60^\circ$ . In addition, this prediction can be proved by the bistetracene derivatives, whose structures can be controlled by different linkers and functional groups of the monomer.

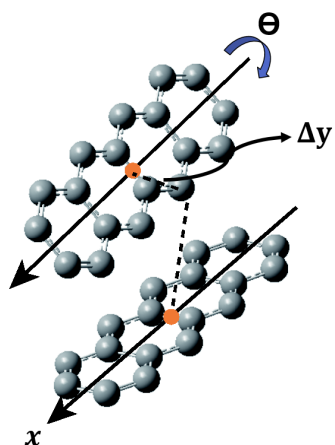


Figure 3.7: Illustration of a tetracene dimer with one monomer is rotated  $\theta$  and shifted  $\Delta y$ . Other parameters are  $\Delta x = 0\text{\AA}$  and  $\Delta z = 4\text{\AA}$ .

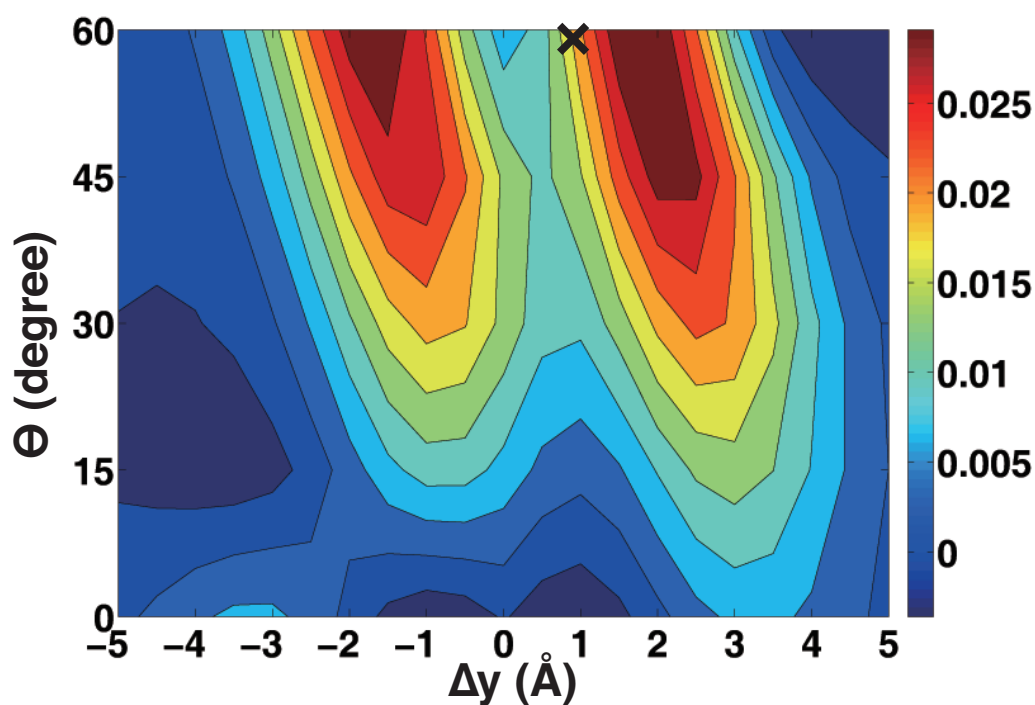


Figure 3.8: 2-D mapping of  $\langle h_B | l_A \rangle$  in a tetracene dimer as functions  $\theta$  and shifted  $\Delta y$ . Other parameters are  $\Delta x = 0\text{\AA}$  and  $\Delta z = 4\text{\AA}$ .







## Chapter 4

### Conclusion

In this work we have investigated the dependence of the basis sets and the size of the active space on the SF effective hamiltonian. In the SF hamiltonian, the diabatic state energies depends a lot on the size of active space. These results implies that the four-orbital-four-electron model can not sufficiently describe the dynamics of the SF process for the energy gaps between diabatic states may not be correct. In addition, from the introduction of the second order perturbation theory, the balance of the static and dynamic correlation is believed to play an important role to properly describe the diabatic state energies of the effective SF hamiltonian.

On the other hand, the size of active space affect little on the couplings in the effective hamiltonian. An imortant insight is that the diabtic state couplings are dominated by the key configurational couplings. This special property allows us to apply HOMO-LUMO basis approximation to evaluating diabatic state couplings for singlet fission process.

Since  $\langle \psi_{TT} | H | \psi_{CT} \rangle$ , which we focus on is dominated by configurational couplings,  $\langle TT | H | CT \rangle$  and  $\langle S_1 S_1 | H | CT \rangle$ , and the diabatic state couplings can be expanded as two electron integrals which are strongly correlated with monomeric orbital overlap  $\langle h_B | l_A \rangle$ . We propose that the couplings,  $\langle TT | H | CT \rangle$  and  $\langle S_1 S_1 | H | CT \rangle$ , can be elucidated by overlap,  $\langle h_B | l_A \rangle$ .

In addition, the dependence of geometrical change on SF couplings are investigated in three different dimer systems. The geometrical change contains the contributions of slip distance and intermolecular orientation, and these contributions are easily identified.

Either the dependence of the slip distance on the couplings in three dimer systems or the dependence of the intermolecular orientation on couplings in tetracene can be successfully elucidated by the overlap. For we didn't impose any extra condition on our theory, we believe that this method can be applied to any other acene dimer systems.

Furthermore, the successful results allow us to regard the overlap as a criterion to predict the optimal geometries for highly efficient SF in a given dimer system. Note that, we mainly focus on how diabatic state couplings are affected by the geometrical change and we didn't discuss any dependence of the geometrical changes on the energy gap between  $\psi_{FE}$  and  $\psi_{TT}$ . Though the energy matching is also a vital condition for efficient SF process, the condition is fully described by Ratner et. al [40, 41].

Finally, we emphasize that the methods presented in this work can provide useful information for molecular design in SF dye-sensitized solar cells [70–81]. Concerning high performance dye-sensitized solar cells, the monomeric orbital overlap can be served as a guideline to optimize the aggregate morphology of organic chromophores.



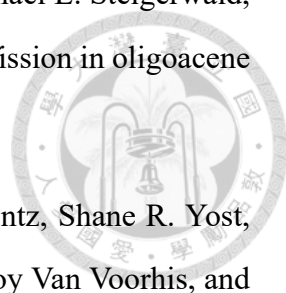
## Bibliography

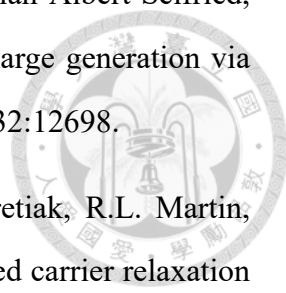
- [1] S. Singh, W. J. Jones, W. Siebrand, B. P. Stoicheff, and W. G. Schneider. Laser generation of excitons and fluorescence in anthracene crystals. *J. Chem. Phys.*, 42:330, 1965.
- [2] Millicent B. Smith and Josef Michl. Singlet fission. *Chem. Rev.*, 110:6891, 2010.
- [3] Millicent B. Smith and Josef Michl. Recent advances in singlet fission. *Acc. Chem. Res.*, 64:361, 2013.
- [4] Akshay Rao, Mark W. B. Wilson, Justin M. Hodgkiss, Sebastian Albert-Seifried, Heinz Bässler, and Richard H. Friend. Exciton fission and charge generation via triplet excitons in pentacene/c60 bilayers. *J. Am. Chem. Soc.*, 132:12698, 2010.
- [5] Millicent B. Smith and Josef Michl. Recent advances in singlet fission. *Ann. Rev. Phys. Chem.*, 64(1), 2013.
- [6] J. Frenkel. On the transformation of light into heat in solids. i. *Phys. Rev.*, 37:17, 1931.
- [7] Charusheela Ramanan, Amanda L. Smeigh, John E. Anthony, Tobin J. Marks, and Michael R. Wasielewski. Competition between singlet fission and charge separation in solution-processed blend films of 6,13-bis(triisopropylsilylethynyl)pentacene with sterically-encumbered perylene-3,4:9,10-bis(dicarboximide)s. *J. Am. Chem. Soc.*, 134:386, 2012.
- [8] Mark W. B. Wilson, Akshay Rao, Bruno Ehrler, and Richard H. Friend. Singlet ex-

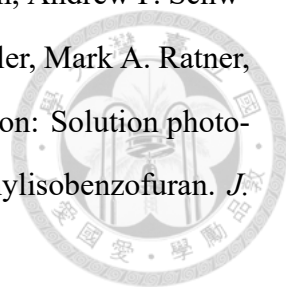
citon fission in polycrystalline pentacene: From photophysics toward devices. *Acc. Chem. Res.*, 46:1330, 2013.



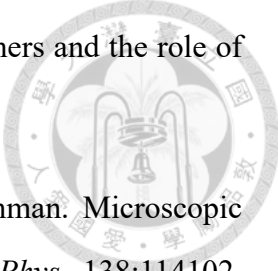
- [9] Jonathan J. Burdett and Christopher J. Bardeen. Quantum beats in crystalline tetracene delayed fluorescence due to triplet pair coherences produced by direct singlet fission. *J. Am. Chem. Soc.*, 134:8597, 2012.
- [10] Andrew F. Schwerin, Justin C. Johnson, Millicent B. Smith, Paiboon Sreearunothai, Duška Popović, Jiří Černý, Zdeněk Havlas, Irina Paci, Akin Akdag, Matthew K. MacLeod, Xudong Chen, Donald E. David, Mark A. Ratner, John R. Miller, Arthur J. Nozik, and Josef Michl. Toward designed singlet fission: Electronic states and photophysics of 1,3-diphenylisobenzofuran. *J. Phys. Chem. A.*, 114:1457, 2010.
- [11] Justin C. Johnson, Arthur J. Nozik, and Josef Michl. High triplet yield from singlet fission in a thin film of 1,3-diphenylisobenzofuran. *J. Am. Chem. Soc.*, 132:16302, 2010.
- [12] Samuel W. Eaton, Leah E. Shoer, Steven D. Karlen, Scott M. Dyar, Eric A. Margulies, Brad S. Veldkamp, Charusheela Ramanan, Daniel A. Hartzler, Sergei Savikhin, Tobin J. Marks, and Michael R. Wasielewski. Singlet exciton fission in polycrystalline thin films of a slip-stacked perylenediimide. *J. Am. Chem. Soc.*, 135:14701, 2013.
- [13] W.G. Albrecht, M.E. Michel-Beyerle, and V. Yakhot. Exciton fission in excimer forming crystal. dynamics of an excimer build-up in  $\alpha$ -perylene. *Chem. Phys.*, 35:193, 1978.
- [14] Ryuzi Katoh and Masahiro Kotani. Fission of a higher excited state generated by singlet exciton fusion in an anthracene crystal. *Chem. Phys. Lett.*, 196:108, 1992.
- [15] H. Najafov, B. Lee, Q. Zhou, L. C. Feldman, and V. Podzorov. Observation of long-range exciton diffusion in highly ordered organic semiconductors. *Nat. Mater.*, 9:938, 2010.

- 
- [16] Samuel N. Sanders, Elango Kumarasamy, Andrew B. Pun, Michael L. Steigerwald, Matthew Y. Sfeir, and Luis M. Campos. Intramolecular singlet fission in oligoacene heterodimers. *Angew. Chem. Int. Edit.*, 55, 2016.
- [17] Daniel N. Congreve, Jiye Lee, Nicholas J. Thompson, Eric Hontz, Shane R. Yost, Philip D. Reuswig, Matthias E. Bahlke, Sebastian Reineke, Troy Van Voorhis, and Marc A. Baldo. External quantum efficiency above 100% in a singlet-exciton-fission-based organic photovoltaic cell. *Sci.*, 340:334, 2013.
- [18] William Shockley and Hans J. Queisser. Detailed balance limit of efficiency of p-n junction solar cells. *J. Appl. Phys.*, 32:510, 1961.
- [19] M. C. Hanna and A. J. Nozik. Solar conversion efficiency of photovoltaic and photoelectrolysis cells with carrier multiplication absorbers. *J. Appl. Phys.*, 100:074510, 2006.
- [20] Wai-Lun Chan, Timothy C. Berkelbach, Makenzie R. Provorse, Nicholas R. Monahan, John R. Tritsch, Mark S. Hybertsen, David R. Reichman, Jiali Gao, and X.-Y. Zhu. The quantum coherent mechanism for singlet fission: Experiment and theory. *Acc. Chem. Res.*, 46:1321, 2013.
- [21] Justin C. Johnson, Arthur J. Nozik, and Josef Michl. The role of chromophore coupling in singlet fission. *Acc. Chem. Res.*, 46:1290, 2013.
- [22] Paul M. Zimmerman, Charles B. Musgrave, and Martin Head-Gordon. A correlated electron view of singlet fission. *Acc. Chem. Res.*, 46:1339, 2013.
- [23] C. Jundt, G. Klein, B. Sipp, J. Le Moigne, M. Joucla, and A.A. Villaeys. Exciton dynamics in pentacene thin films studied by pump-probe spectroscopy. *Chem. Phys. Lett.*, 241:84, 1995.
- [24] Akshay Rao, Mark W. B. Wilson, Sebastian Albert-Seifried, Riccardo Di Pietro, and Richard H. Friend. Photophysics of pentacene thin films: The role of exciton fission and heating effects. *Phys. Rev. B*, 84:195411, 2011.

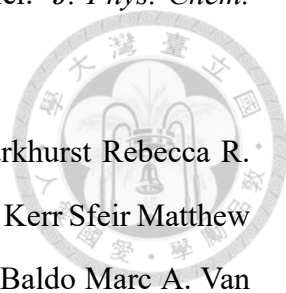
- 
- [25] Akshay Rao, Mark W. B. Wilson, Justin M. Hodgkiss, Sebastian Albert-Seifried, Heinz Bäessler, and Richard H. Friend. Exciton fission and charge generation via triplet excitons in pentacene/c60 bilayers. *J. Am. Chem. Soc.*, 132:12698.
- [26] V.K. Thorsmølle, R.D. Averitt, J. Demsar, D.L. Smith, S. Tretiak, R.L. Martin, X. Chi, B.K. Crone, A.P. Ramirez, and A.J. Taylor. Photoexcited carrier relaxation dynamics in pentacene probed by ultrafast optical spectroscopy: Influence of morphology on relaxation processes. *Phys. B*, 404:3127, 2009.
- [27] Thomas S. Kuhlman, Jacob Kongsted, Kurt V. Mikkelsen, Klaus B. Møller, and Theis I. Sølling. Interpretation of the ultrafast photoinduced processes in pentacene thin films. *J. Am. Chem. Soc.*, 132:3431, 2010.
- [28] Mark W. B. Wilson, Akshay Rao, Jenny Clark, R. Sai Santosh Kumar, Daniele Brida, Giulio Cerullo, and Richard H. Friend. Ultrafast dynamics of exciton fission in polycrystalline pentacene. *J. Am. Chem. Soc.*, 133:11830, 2011.
- [29] Lin Ma, Keke Zhang, Christian Kloc, Handong Sun, Maria E. Michel-Beyerle, and Gagik G. Gurzadyan. Singlet fission in rubrene single crystal: direct observation by femtosecond pump-probe spectroscopy. *Phys. Chem. Chem. Phys.*, 14:8307, 2012.
- [30] Henning Marciniak, Igor Pugliesi, Bert Nickel, and Stefan Lochbrunner. Ultrafast singlet and triplet dynamics in microcrystalline pentacene films. *Phys. Rev. B*, 79:235318, 2009.
- [31] Astrid M. Müller, Yuri S. Avlasevich, Klaus Müllen, and Christopher J. Bardeen. Evidence for exciton fission and fusion in a covalently linked tetracene dimer. *Chem. Phys. Lett.*, 421:518, 2006.
- [32] Jonathan J. Burdett and Christopher J. Bardeen. The dynamics of singlet fission in crystalline tetracene and covalent analogs. *Acc. Chem. Res.*, 46:1312, 2013.
- [33] Heyuan Liu, Xuemin Wang, Lingyun Pan, Li Shen, Xiangyang Wang, Qidai Chen, and Xiyu Li. Synthesis and photophysical properties of a bistetracene compound with slipped stacked structure. *J. Photoch. Photobio. A*, 340:21, 2017.

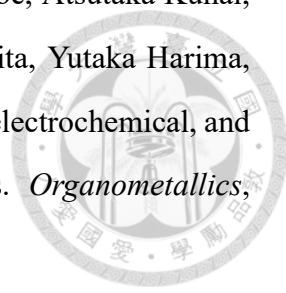
- 
- [34] Justin C. Johnson, Akin Akdag, Matibur Zamadar, Xudong Chen, Andrew F. Schwerin, Irina Paci, Millicent B. Smith, Zdeněk Havlas, John R. Miller, Mark A. Ratner, Arthur J. Nozik, and Josef Michl. Toward designed singlet fission: Solution photo-physics of two indirectly coupled covalent dimers of 1,3-diphenylisobenzofuran. *J. Phys. Chem. B*, 117:4680, 2013.
- [35] Zirzmeier Johannes Hetzer Constantin Phelan Brian T. Krzyaniak Matthew D. Reddy S. Rajagopala Coto Pedro B. Horwitz Noah E. Young Ryan M. White Fraser J. Hampel Frank Clark Timothy Thoss Michael Tykwinski Rik R. Wasielewski Michael R. Basel, Bettina S. and Dirk M. Guldi. Unified model for singlet fission within a non-conjugated covalent pentacene dimer. *Sci. Comm.*, 8:15171, 2017.
- [36] Paul M. Zimmerman, Zhiyong Zhang, and Charles B. Musgrave. Singlet fission in pentacene through multi-exciton quantum states. *Nat. Chem.*, 2:648, 2010.
- [37] L. Sebastian, G. Weiser, and H. Bassler. Charge transfer transitions in solid tetracene and pentacene studied by electroabsorption. *Chem. Phys.*, 61:125, 1981.
- [38] N.E. Geacintov, J. Burgos, M. Pope, and C. Strom. Heterofission of pentacene excited singlets in pentacene-doped tetracene crystals. *Chem. Phys. Lett.*, 11:504, 1971.
- [39] Y. Tomkiewicz, R. P. Groff, and P. Avakian. Spectroscopic approach to energetics of exciton fission and fusion in tetracene crystals. *J. Chem. Phys.*, 54:4504, 1971.
- [40] Eric C. Greyson, Josh Vura-Weis, Josef Michl, and Mark A. Ratner. Maximizing singlet fission in organic dimers: Theoretical investigation of triplet yield in the regime of localized excitation and fast coherent electron transfer. *J. Phys. Chem. B*, 114:14168, 2010.
- [41] Eric C. Greyson, Brian R. Stepp, Xudong Chen, Andrew F. Schwerin, Irina Paci, Millicent B. Smith, Akin Akdag, Justin C. Johnson, Arthur J. Nozik, Josef Michl, and Mark A. Ratner. Singlet exciton fission for solar cell applications: Energy aspects of interchromophore coupling. *J. Phys. Chem. B*, 114:14223, 2010.

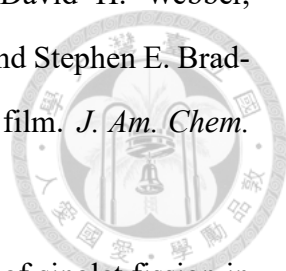


- 
- [42] Timothy C. Berkelbach, Mark S. Hybertsen, and David R. Reichman. Microscopic theory of singlet exciton fission. ii. application to pentacene dimers and the role of superexchange. *J. Chem. Phys.*, 138(11), 2013.
- [43] Timothy C. Berkelbach, Mark S. Hybertsen, and David R. Reichman. Microscopic theory of singlet exciton fission. i. general formulation. *J. Chem. Phys.*, 138:114102, 2013.
- [44] Paul E. Teichen and Joel D. Eaves. A microscopic model of singlet fission. *J. Phys. Chem. B*, 116:11473, 2012.
- [45] N. Monahan and X.-Y. Zhu. Charge transfer-mediated singlet fission. *Acc. Chem. Res.*, 66:601, 2015.
- [46] Fatemeh Mirjani, Nicolas Renaud, Natalie Gorczak, and Ferdinand C. Grozema. Theoretical investigation of singlet fission in molecular dimers: The role of charge transfer states and quantum interference. *J. Phys. Chem. C.*, 118:14192, 2014.
- [47] Nicolas Renaud, Paul A. Sherratt, and Mark A. Ratner. Mapping the relation between stacking geometries and singlet fission yield in a class of organic crystals. *J. Phys. Chem. Lett.*, 4:1065, 2013.
- [48] Remco W.A. Havenith, Hilde D. de Gier, and Ria Broer. Explorative computational study of the singlet fission process. *Mol. Phys.*, 110:2445, 2012.
- [49] Ethan C. Alguire, Joseph E. Subotnik, and Niels H. Damrauer. Exploring non-condon effects in a covalent tetracene dimer: How important are vibrations in determining the electronic coupling for singlet fission? *J. Phys. Chem. A*, 119:299, 2015.
- [50] Xintian Feng, Anatoliy V. Luzanov, and Anna I. Krylov. Fission of entangled spins: An electronic structure perspective. *J. Phys. Chem. Lett.*, 4:3845, 2013.
- [51] Eric C. Greyson, Josh Vura-Weis, Josef Michl, and Mark A. Ratner. Maximizing singlet fission in organic dimers: Theoretical investigation of triplet yield in the

regime of localized excitation and fast coherent electron transfer. *J. Phys. Chem. B*, 114:14168, 2010.

- 
- [52] Lee Jiye Wilson Mark W. B. Wu Tony McMahon David P. Parkhurst Rebecca R. Thompson Nicholas J. Congreve Daniel N. Rao Akshay Johnson Kerr Sfeir Matthew Y. Bawendi Mounqi G. Swager Timothy M. Friend Richard H. Baldo Marc A. Van Voorhis Troy Yost, Shane R. A transferable model for singlet-fission kinetics. *Nat. Chem.*, 6:492, 2014.
- [53] Attila Szabo and Neil S. Ostlund. *Modern quantum chemistry: Introduction to advanced electronic structure theory*. 1996.
- [54] Naoto Ishikawa, Osamu Ohno, Youkoh Kaizu, and Hiroshi Kobayashi. Localized orbital study on the electronic structure of phthalocyanine dimers. *J. Phys. Chem.*, 96(22):8832, 1992.
- [55] David Yaron. Nonlinear optical response of conjugated polymers: Essential excitations and scattering. *Phys. Rev. B*, 54:4609, 1996.
- [56] T. Pacher, L. S. Cederbaum, and H. Köppel. Approximately diabatic states from block diagonalization of the electronic hamiltonian. *J. Chem. Phys.*, 89:7367–7381, 1988.
- [57] Benoit Champagne, Denis Jacquemin, Jean-Marie André, and Bernard Kirtman. Ab initio coupled hartree-fock investigation of the static first hyperpolarizability of model all-trans-polymethineimine oligomers of increasing size. *J. Phys. Chem. A*, 101:3158, 1997.
- [58] Benoit Champagne, Milena Spassova, Jean-Benoit Jadin, and Bernard Kirtman. Ab initio investigation of doping-enhanced electronic and vibrational second hyperpolarizability of polyacetylene chains. *J. Chem. Phys.*, 116:3935, 2002.
- [59] Yirong Mo, Wei Wu, and Qianer Zhang. Theoretical resonance energies of benzene, cyclobutadiene, and butadiene. *J. Phys. Chem.*, 98:10048, 1994.

- 
- [60] Joji Ohshita, Mitsunori Nodono, Hiroyuki Kai, Tsuguo Watanabe, Atsutaka Kunai, Kenji Komaguchi, Masaru Shiotani, Akira Adachi, Koichi Okita, Yutaka Harima, Kazuo Yamashita, and Mitsuo Ishikawa. Synthesis and optical, electrochemical, and electron-transporting properties of silicon-bridged bithiophenes. *Organometallics*, 18:1453, 1999.
- [61] Miquel Torrent-Sucarrat, Miquel Sol, Miquel Duran, Josep M. Luis, and Bernard Kirtman. Basis set and electron correlation effects on ab initio electronic and vibrational nonlinear optical properties of conjugated organic molecules. *J. Chem. Phys.*, 118:711, 2003.
- [62] Giorgio Orlandi, Paolo Palmieri, Riccardo Tarroni, Francesco Zerbetto, and Marek Z. Zgierski. The s<sub>0</sub>(1ag) s<sub>1</sub>(1b2u) vibronic transition in benzene: An ab initio study. *J. Chem. Phys.*, 100:2458, 1994.
- [63] Denis Jacquemin, Benoit Champagne, and Christof Hättig. Correlated frequency-dependent electronic first hyperpolarizability of small push-pull conjugated chains. *Chem. Phys. Lett.*, 319:327, 2000.
- [64] Roos. B, Per Linse, Per E.M. Siegbahn, and Margareta R.A. Blomberg. A simple method for the evaluation of the second-order-perturbation energy from external double-excitations with a casscf reference wavefunction. *Chem. Phys.*, 66:197, 1982.
- [65] Kerstin. Andersson, Per Aake. Malmqvist, Bjoern O. Roos, Andrzej J. Sadlej, and Krzysztof. Wolinski. Second-order perturbation theory with a casscf reference function. *J. Phys. Chem.*, 94:5483, 1990.
- [66] K. Andersson. Different forms of the zeroth-order hamiltonian in second-order perturbation theory with a complete active space self-consistent field reference function. *Theor. Chimica. Acta.*, 91:31, 1995.
- [67] N. O. Lipari and C. B. Duke. The electronic structure of polyacenes: Naphthalene through pentacene. *J. Chem. Phys.*, 63, 1975.

- 
- [68] Sean T. Roberts, R. Eric McAnally, Joseph N. Mastron, David H. Webber, Matthew T. Whited, Richard L. Brutchey, Mark E. Thompson, and Stephen E. Bradforth. Efficient singlet fission discovered in a disordered acene film. *J. Am. Chem. Soc.*, 134:6388, 2012.
- [69] Karan Aryanpour, Alok Shukla, and Sumit Mazumdar. Theory of singlet fission in polyenes, acene crystals, and covalently linked acene dimers. *J. Phys. Chem. C.*, 119, 2015.
- [70] Xuejun Zhang, Ying Zhu, Xiaobo Wu, Huipeng He, Gaolei Wang, and Qiaoling Li. Meso-schiff-base substituted porphyrin dimer dyes for dye-sensitized solar cells: synthesis, electrochemical, and photovoltaic properties. *Res. Chem. Intermed.*, 41:4227, 2015.
- [71] Tao Zhang, Xing Qian, Peng-Fei Zhang, Yi-Zhou Zhu, and Jian-Yu Zheng. A meso-meso directly linked porphyrin dimer-based double d-[small pi]-a sensitizer for efficient dye-sensitized solar cells. *Chem. Commun.*, 51:3782–3785, 2015.
- [72] Tomofumi Hamamura, Joanne Ting Dy, Koichi Tamaki, Jotaro Nakazaki, Satoshi Uchida, Takaya Kubo, and Hiroshi Segawa. Dye-sensitized solar cells using ethynyl-linked porphyrin trimers. *Phys. Chem. Chem. Phys.*, 16:4551, 2014.
- [73] Ximena Zarate, Francisca Claveria-Cadiz, David Arias-Olivares, Angela Rodriguez-Serrano, Natalia Inostroza, and Eduardo Schott. Effects of the acceptor unit in dyes with acceptor-bridge-donor architecture on the electron photo-injection mechanism and aggregation in dsscs. *Phys. Chem. Chem. Phys.*, 18:24239, 2016.
- [74] Yousuke Ooyama, Koji Uenaka, Takuya Kamimura, Shuwa Ozako, Masahiro Kanda, Taro Koide, and Fumito Tani. Dye-sensitized solar cell based on an inclusion complex of a cyclic porphyrin dimer bearing four 4-pyridyl groups and fullerene c60. *RSC Adv.*, 6:16150, 2016.
- [75] Kenji Sunahara, Matthew J. Griffith, Takayuki Uchiyama, Pawel Wagner, David L. Officer, Gordon G. Wallace, Attila J. Mozer, and Shogo Mori. A nonconjugated

bridge in dimer-sensitized solar cells retards charge recombination without decreasing charge injection efficiency. *ACS Appl. Mater. Interfaces*, 5:10824, 2013.

- [76] Emi Nakano, Katsuya Mutoh, Yoichi Kobayashi, and Jiro Abe. Electrochemistry of photochromic [2.2]paracyclophane-bridged imidazole dimers: Rational understanding of the electronic structures. *J. Phys. Chem. A*, 118:2288, 2014.
- [77] Hitoshi Kusama and Kazuhiro Sayama. Theoretical study on the intermolecular interactions of black dye dimers and black dye-deoxycholic acid complexes in dye-sensitized solar cells. *J. Phys. Chem. C*, 116:23906, 2012.
- [78] Nicholas A. Treat, Fritz J. Knorr, and Jeanne L. McHale. Templated assembly of betanin chromophore on tio<sub>2</sub>: Aggregation-enhanced light-harvesting and efficient electron injection in a natural dye-sensitized solar cell. *J. Phys. Chem. C*, 120:9122, 2016.
- [79] Fujimoto Junko, Manseki Kazuhiro, and Miyaji Hidekazu. Dye-sensitized solar cells using supramolecular porphyrin arrays inspired by  $\pi$ -stacking structures of photosynthetic light-harvesting complexes. *Chem. Lett.*, 43:207, 2014.
- [80] Tomohiro Higashino, Kenichi Sugiura, Yukihiro Tsuji, Shimpei Nimura, Seigo Ito, and Hiroshi Imahori. A push-pull porphyrin dimer with multiple electron-donating groups for dye-sensitized solar cells: Excellent light-harvesting in near-infrared region. *Chem. Lett.*, 45:1126, 2016.
- [81] Thibaud Etienne, Laurent Chbib, Catherine Michaux, Eric A. Perpète, Xavier Assfeld, and Antonio Monari. All-organic chromophores for dye-sensitized solar cells: A theoretical study on aggregation. *Dyes. Pigm.*, 101:203, 2014.